Results in Engineering 30 (2026) 110386

Contents lists available at ScienceDirect

Results in Engineering

journal homepage: www.sciencedirect.com/journal/results-in-engineering

Research paper

Parametric energy and exergy evaluation of a new hybrid photovoltaic thermal system using 3D computational analysis

Yassine El Alami [a,*], Mohamed El Habib Amagour [b], Rehena Nasrin [c], Fatima Majid [d], Redouane Rmaily [a], Elhadi Baghaz [a], Khaled M. Al-Aribe [e], Adnan Ibrahim [f,*]

[a] Laboratory of Electronics, Instrumentation and Energetic, Faculty of Sciences, Chouaïb Doukkali University, B.P 20, El Jadida, Morocco
[b] Green Energy Park, IRESEN-UM6P, Km 2 Route Régionale R206, Benguerir, Morocco
[c] Department of Mathematics, Bangladesh University of Engineering and Technology, Dhaka, Bangladesh
[d] Laboratory of Nuclear, Atomic, Molecular, Mechanical and Energetic Physics Department, Faculty of Science, Chouaïb Doukkali University, B.P.20, El Jadida, Morocco
[e] Department of Mechanical and Industrial Engineering, Abu Dhabi University, Abu Dhabi PO Box 59911, United Arab Emirates
[f] Solar Energy Research Institute, Universiti Kebangsaan Malaysia, 43600, Bangi, Selangor, Malaysia

ARTICLE INFO

Keywords:
Channel-shaped HE
Energy and exergy analysis
FEM
Numerical simulation
Photovoltaic thermal system

ABSTRACT

In light of recent advances, two main gaps persist in the literature: limited studies on box-type photovoltaic-thermal systems (PVT-S) and the absence of surface temperature dispersal analyses. Selecting suitable heat exchanger (HE) materials compatible with the system's architecture is essential. To address these gaps, this study introduces a new PVT-S configuration. Energy and exergy performances were evaluated under varying operating conditions, including mass flow rate (FR), inlet temperature of the heat transfer (HT) fluid, and solar irradiation. Three-dimensional simulations were performed in COMSOL Multiphysics® using the finite element method (FEM), and the numerical approach was validated against experimental and numerical data from the literature. The results show that copper and aluminum have similar HE performance, suggesting that aluminum is a lighter and more cost-effective alternative. Increased solar radiation generally improved PVT-S efficiency, although electrical efficiency (EE) decreased slightly by 0.34% and reached a maximum value of 12.29%. The maximum thermal efficiency (TE) achieved by the system is 80.9%, and the exergy efficiency is 15.6%. Higher FRs improve energy yields but reduce exergy-based yields. Increasing the inlet temperature reduces both electrical (-0.53%) and thermal (-11.56%) yields, while improving total thermal and exergy yields, but decreasing electrical exergy yield.

1. Introduction

The increasing global population, combined with ongoing industrial development, presents a significant challenge in meeting energy demands. However, the intensive use of fossil fuels as the primary energy source has had severe consequences, including acid rain, global warming, rapid climate change, and devastating impacts on human health and the environment [1]. These effects have even led to the extinction of certain animal species. To address these issues, the transition to clean, environmentally friendly energy sources has become an unavoidable strategy [2,3]. Solar energy is currently considered one of the best alternatives, drawing significant interest because of its abundance and its environmentally sustainable characteristics [4–6]. This energy source is used in a variety of applications in our daily lives, ranging from water heating to electricity generation. Photovoltaic (PV) technologies occupy a prominent place among the applications exploiting this resource [7–9]. PV panels convert only a fraction of the incident solar radiation into electrical energy (typically between 15 and 25%) [10]. The remaining portion of this energy is either reflected or dissipated as heat within the module, leading to an increase in the temperature of the PV cells [11]. This, in turn, reduces EE and shortens the lifespan of the solar cells [12–14]. PVT-Ss are emerging as a promising solution for harnessing solar energy more efficiently by combining thermal energy collection with electrical power generation [15,16]. Since the PVT-S was first conceived in 1970 [17], intensive research into these hybrid systems has continued to progress.

The performance of PVT-Ss is likely to be influenced by various parameters, including design, operating, and climatic parameters [18,19]. Over the last decade, various design approaches have been considered to

* Corresponding authors.
E-mail addresses: yassineelalami97@gmail.com (Y. El Alami), iadnan@ukm.edu.my (A. Ibrahim).

https://doi.org/10.1016/j.rineng.2026.110386
Received 26 February 2026; Received in revised form 23 March 2026; Accepted 3 April 2026
Available online 3 April 2026

Nomenclature

Parameters

T_{ted}	Tedlar temperature (°C)
T_{sun}	Surface temperature of the sun (°C)
E_{loss}	Overall energy losses (W)
$\dot{X}_{th}$	Thermal exergy (W)
T_g	Glass temperature (°C)
$\dot{m}$	Volume flow rate (L/h)
T_{out}	Temperature of output water (°C)
$c_{p,f}$	Specific heat (J kg^{-1}K^{-1})
E_p	Electrical power (W)
E_{in}	Energy input to the solar cell (W)
E_{th}	Thermal energy (W)
p_c	Packing factor (%)
T_r	Reference temperature (°C)
T_c	Temperature of the solar cell (°C)
k	Thermal conductivity (W m^{-1} K^{-1})
T_s	Temperature of the surface (°C)
v_{in}	Water inlet velocity (m/s)
u, v, w	Velocity components (m/s)
n	Surface normal
$\dot{X}_{el}$	Electrical exergy (W)
$\dot{X}_{sun}$	Solar exergy input to the PVT system

Greek symbols

η_{th}	Thermal efficiency (%)
η_{ref}	PV efficiency (at STC conditions)
τ_g	Glass transmissivity
ρ	Density (kg m^{-3})
ε_{th}	Thermal exergy efficiency (%)
η_g	Overall efficiency (%)
η_{el}	Electrical efficiency (%)
ε_g	Glass emissivity
α_{sc}	Solar cell absorptivity
$\varepsilon_{overall}$	Overall exergy efficiency (%)
ε_{el}	Electrical exergy efficiency (%)

Abbreviations

EEX	Electrical exergy
EE	Electrical efficiency
FR	Flow rate
FEM	Finite element method
OE	Overall efficiency
PVT-S	Photovoltaic thermal system
PV	Photovoltaic
TEX	Thermal exergy
TE	Thermal efficiency
HE	Heat exchanger

maximize the efficiency of PVT-Ss, with particular emphasis on optimizing the shapes of the heat absorbers and the structural configurations of the cooling channels. Hussain et al. [20] performed an experimental investigation on a PVT-S cooling channel featuring hexagonal fins. Their results showed an approximate 0.2% increase in EE alongside a 20 to 70% enhancement in TE. El Alami et al. [21] studied a new PVT-S with water directly attached to the PV rear, showing improved temperature uniformity, lower pressure loss, higher energy and exergy efficiencies (75.83% and 17.56%), and enhanced sustainability indicators compared to conventional PV systems. Ozakin [22] investigated and compared the energy efficiency of three different cooling channel configurations: empty channels, channels with closely spaced fins, and channels with sparsely distributed fins. The results show that with sparse fins, the exergy efficiency increased by around 70%, while with frequent fins it increased by 30% compared with the empty state. Emam et al. [23] studied a water-based PVT-S with PCM capsules, showing that it reduced cell temperature, increased EE and power output, achieved overall efficiencies up to 67.33% with a peak exergy efficiency of 74.64%, shortened payback to 1.58 years, and reduced carbon emissions by 32% compared to uncooled PV panels. Misha et al. [24] introduced a water-cooled PVT-S featuring a novel double oscillation absorber. The research integrated CFD modeling via ANSYS 19.2 with experiments conducted under Malaysian climatic conditions. Results at a mass FR of 6 L/min indicated a maximum EE of 11.71% and an average TE reaching 59.6%. Nahar et al. [25] proposed a novel spiral flow channel design tailored for PVT-Ss. This channel was bonded directly to the PV module using thermal paste and tested with both aluminum and copper tubes. Their findings revealed nearly identical performance between the two materials. Furthermore, the implementation of the flow channel described by Nahar et al. [25] achieved a panel temperature reduction of 42 °C, which corresponded to a 2% increase in the EE of the PV module. Refaey et al. [26] studied the thermal regulation of solar panels using PCMs. Three PCMs (RT31, RT35, RT42) were tested with different fin geometries. The RT31 proved unsuitable due to its low melting point. When using RT35 and RT42 under irradiance levels ranging from 510 to 850 W/m^2, RT42 with triangular fins reduced the panel temperature by 19.4 to 24% compared to uncooled panels, thereby increasing efficiency by 7 to 8.4%. The RT42 also demonstrated a longer service life and faster solidification overnight, thereby improving overall thermal performance. Yu et al. [27] focused on the impact of channel design on PVT-S performance by comparing two absorber plate types connected via rollers. Their study revealed that the PVT-S equipped with a grid channel achieved higher electrical and thermal efficiencies than the one using a harp channel. Hamada et al. [28] studied an innovative water-based PVT-S incorporating PCM capsules, capable of operating in both active and passive cooling modes. Experiments conducted under real-world outdoor conditions in Cairo showed that, with a water FR of 3 L/min, the actively cooled PVT-PCM panel achieved a maximum overall efficiency (OE) of 74.1%, compared to 34.6% for the passively cooled panel and 12% for a reference air-cooled PV panel, thus demonstrating significant improvements in both electricity generation and thermal energy storage. De Luca et al. [29] investigated an innovative flat-plate PVT-S through numerical modeling. Their design incorporates vacuum layers placed either above or below the PV panel. According to their results, this setup greatly minimizes convective heat loss and notably enhances both the energy and exergy performance of the system. Sheshpoli et al. [30] combined numerical simulations and experiments to assess various PVT-S designs, with the goal of finding the optimal cooling tube layout. Their analysis revealed that certain configurations exhibited higher temperatures than the reference setup. Upon determining the most efficient arrangement, they implemented it in northern Iran, where the system showed a marked increase in TE (48.4%) and EE (7.3%) compared to panels without cooling. El Alami et al. [31] studied a PVT-S cooled using nanofluids containing copper nanoparticles (Cu NP). The blade-shaped nanoparticles increased TE from 3.2% to 3.6% and raised exergetic efficiency to 15.35%, with annual energy and exergy outputs of 2672.09 kWh and 515.76 kWh. Higher irradiance improved durability, demonstrating that Cu NP-based nanofluids and optimized geometry enhance the performance of the PVT-S and the overall durability of the system. Mohammadi et al. [32] analyzed a PVT-S using a flattened-tube HE combined with PCM and nanofluid. They showed that a 44% tube flattening, with a silver-based nanofluid (10%), achieves a PV temperature of 54.04 °C and good thermal uniformity, but at the cost of increased pressure drop and reduced PCM melting. Madadi et al. [33]

proposed a novel PVT-S integrating flat heat sinks and serpentine copper tubes enclosed in a paraffin wax-filled sealed container, attached to the rear of the PV panel. The system was tested experimentally using water, SiC/water, and graphene/water nanofluids at 0.2% and 0.4% concentrations and FRs of 0.5 and 1 L/min. Results showed that nanofluids, especially graphene-based ones, significantly reduced PV temperature and improved both electrical and thermal efficiencies compared to water and the uncooled PV panel. Radhi et al. [34] developed an innovative PVT-S collector incorporating a square spring, micro-fin tube, and twisted tape, combined with Al_2O_3-based nanofluids and nanophase change materials. Tested under a solar simulator with irradiance up to 1000 W/m^2 and FRs from 0.016 to 0.05 kg/s, the system achieved peak thermal and electrical efficiencies of 86.5 % and 13.171%, respectively. Compared to a conventional PV panel, it yielded a 39.24 % increase in EE by lowering the cell temperature from 77.8 °C to 35.7 °C. Kazemian et al. [35] investigated PVT-S using a wavy HE tube, optimizing five key design parameters. The results showed that the wavy configuration significantly enhanced energy (85%) and exergy (14.67%) efficiencies compared to the straight-tube design, confirming the effectiveness of this geometry for solar applications.

Flat plate PVT-S (wave collectors, serpentine collectors, etc.) [33–35] are the most commonly used due to their simple design and relatively low cost. However, they present several significant issues. One of the main problems is thermal inhomogeneity caused by imperfect contact between the cooling tubes and the panel plate, leading to an uneven temperature profile on the PV panel surface. This temperature variation reduces the EE of the panel and can accelerate its degradation. Additionally, HT in these systems is often limited by the small heat exchange surface provided by the flat tubes and by irregular fluid flow, which lowers cooling efficiency. Moreover, hydraulic pressure losses can be high at elevated FRs, and the system may struggle to maintain optimal temperature under high solar irradiance. In comparison, box-type or channel-based PVT-Ss (Fig. 1) offer several advantages. Their design allows for the integration of wide or multiple channels, ensuring better circulation and more uniform distribution of the HT fluid. This configuration improves HT by increasing the contact surface between the fluid and the hot surface, resulting in more effective and uniform cooling of the PV panel. Box-type systems also offer better management of pressure losses, as the fluid can circulate more freely through wider or optimized flow passages.

In light of the most recent advances, the authors note that the literature on waterborne PVT-Ss still has some shortcomings. Few studies [36–38] have focused on channel box configurations, despite their potential effectiveness. Furthermore, detailed data on collector surface temperature variation and pressure losses in this type of design remain limited.

The study intends to design an innovative thermal exchanger of channel-box architecture, specifically developed to enhance convective transfers within the system. This new structure is characterized by its innovative design, in which almost the entire surface of the PV panel is in direct contact with the HT fluid. This configuration maximizes the contact surface, unlike traditional PVT-S sheet-and-tube systems

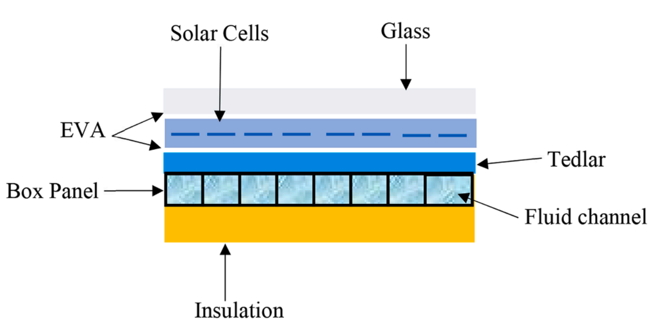

Fig. 1. channel-box PVT-S.

[33–35], where contact between the sheet and the tube is limited, making HT less efficient. In addition, this proposal addresses the problem of uneven temperatures across the panel surface. Conventional systems often have large temperature gradients, which can lead to thermal variations and stresses on the PV cells, affecting their performance and durability. The new structure aims to even out the temperature across the entire surface of the panel, reducing the risk of premature degradation of PV panels and increasing their lifetime.

This work provides the following significant contributions:

- Investigation of the impact of different parameters, such as FR, inlet water temperature, and varying levels of solar irradiation, on the energy and exergy performance of the proposed PVT-S.
- Analysis of the materials used in the manufacture of the HE to identify the most appropriate for the proposed system and for other PVT-Ss.
- Validation of the new system's reliability through comparison with numerical as well as experimental results from existing literature.

This work is structured around four key sections. The first reviews the present situation of knowledge on PVT-Ss. The second part adopts the 3D numerical modeling developed for the study. The third part is results analysis, put into perspective in relation to previously published data. The final section summarizes the main findings and looks ahead to future prospects.

2. Methodology

2.1. Configuration and operating principle

This new system is based on a standard PV panel, composed of several superimposed layers that provide protection, transform solar energy into electrical power, and insulate the module. On the surface, a glass plate provides mechanical protection while allowing light to pass through. Just below, an encapsulation layer, generally made of EVA (ethylene vinyl acetate), holds the solar cells in place. These cells, the heart of the device, are responsible for converting solar radiation into electricity. Finally, another encapsulation layer protects the back of the cells, followed by a sheet of Tedlar, which forms the module's final layer and ensures its thermal stability and resistance to external agents. During operation, however, a large proportion of the solar energy absorbed is converted not into electricity, but into heat. This temperature rise reduces the module's EE. To mitigate this undesirable effect, a HE is attached to the rear of the panel to recover the excess heat and maintain the panel at a moderate temperature. The HE designed for this study features a well-organized internal structure, allowing controlled circulation of a cooling fluid. It consists mainly of a microchannel plate (Fig. 2) that comes into direct contact with the rear face of the PV panel. This plate contains numerous circular channels through which the fluid circulates. Thanks to its thinness, it facilitates rapid HT between the heated panel and the fluid. Additionally, apertures in its bottom wall connect the internal channels to the fluid inlet and outlet zones, ensuring a smooth and balanced distribution throughout the system. The fluid is introduced into the exchanger via a manifold located on one side (Fig. 3). This manifold distributes the liquid throughout the channels. After absorbing the heat, the fluid is recovered by a second collector on the other side of the system. This arrangement ensures even fluid distribution across the entire surface of the plate, enhancing cooling efficiency. In all, the HE comprises 94 channels, carefully arranged to ensure stable circulation, with no stagnant zones, and good heat exchange. The collectors are connected to the outside of the system by simple, seamless fittings, making them easy to integrate into a hydraulic circuit.

This PVT-S was numerically modeled using COMSOL Multiphysics® software, which simulates the interaction between thermal, fluidic, and structural phenomena. The approach adopted is based on solving the

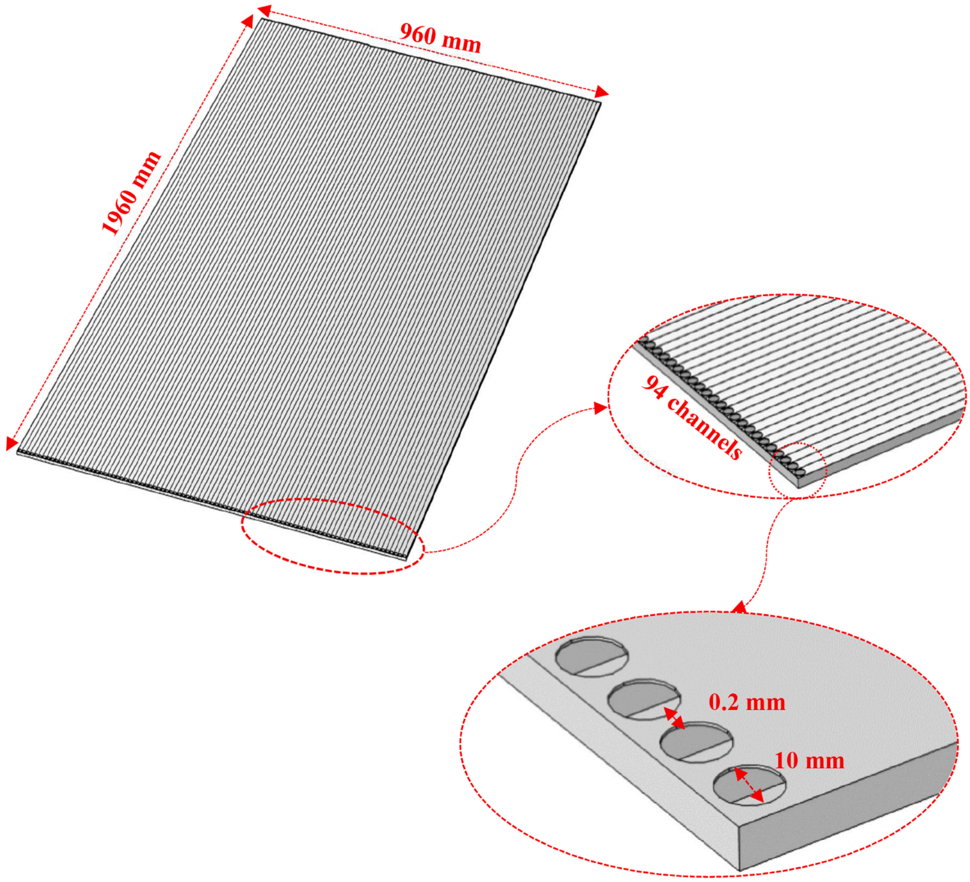

Fig. 2. Detailed view of the microchannel plate with its integrated circular channels at the rear of the PV panel.

physics of conjugate HT, which considers conduction, convection, and fluid flow through the various parts of the system. A flow chart (Fig. 4) illustrating all the steps involved in the numerical simulation, from geometric modeling to analysis of the results, is presented for a better understanding of the computational process. The data were then represented graphically with Origin, and the material properties and geometric parameters used are listed in Tables 1 and 2.

2.2. Key assumptions and fundamental equations

The numerical investigation was conducted within the COMSOL Multiphysics® environment, employing the FEM as the primary approach. The fluid flow was treated as steady, incompressible, and uniformly distributed, falling within the laminar regime. For getting proper thermal and hydrodynamic characteristics, appropriate Multiphysics couplings were applied, particularly those accounting for non-isothermal flow conditions. Several simplifying assumptions were introduced to facilitate the simulation of the PVT-S configuration, among which are the following:

- The EVA encapsulant was assumed to be perfectly transparent, allowing full transmission of incident solar radiation,
- The PVT-S surface was considered clean, without any dust deposition that could alter its solar absorptivity [40],
- All thermophysical properties were expected as constant, irrespective temperature fluctuations [41],
- The temperatures of the sky and the surrounding atmosphere were treated as equivalent in the simulation,
- Heat losses through the edges and the backside of the PVT-S were neglected,
- Ideal thermal contact was assumed between all components of the PVT-S assembly [42].

In the solid components of the PVT-S, HT was primarily modeled as conduction. This process involves the transfer of thermal energy via the vibrational motion of particles within the material. The analysis of heat flow through the PV cell surfaces relies on solving the thermal conduction equation presented below [25,43]:

$$\nabla\cdot(k\nabla T) = 0 \tag{1}$$

The equations governing conjugate heat transfer are accompanied by equations of conservation of mass and momentum, which describe the behavior of the fluid. In COMSOL, these equations are formulated as follows [25,43,44]:

$$\rho C_p\frac{\partial T}{\partial t} + \rho C_p u\cdot\nabla T = \nabla\cdot(k\nabla T) + Q \tag{2}$$

$$\rho\frac{\partial u}{\partial t} + \nabla\cdot(\rho u) = 0 \tag{3}$$

$$\rho\cdot\frac{\partial u}{\partial t} + \rho(u\cdot\nabla)u = \nabla\cdot\left[-pI + \mu\left(\nabla u + (\nabla u)^{\mathrm{T}}\right)\right] + F \tag{4}$$

2.3. Boundary conditions

In the numerical model, the inlet temperature and fluid FR were prescribed as boundary conditions for the fluid circulating within the channels. The outlet pressure was fixed at atmospheric pressure (0 atm). A no-slip condition was imposed on the channel walls. Heat dissipation from the PVT-S occurs through radiation and convection at the glass, whereas the lateral faces were kept insulated (Fig. 5). The glass's

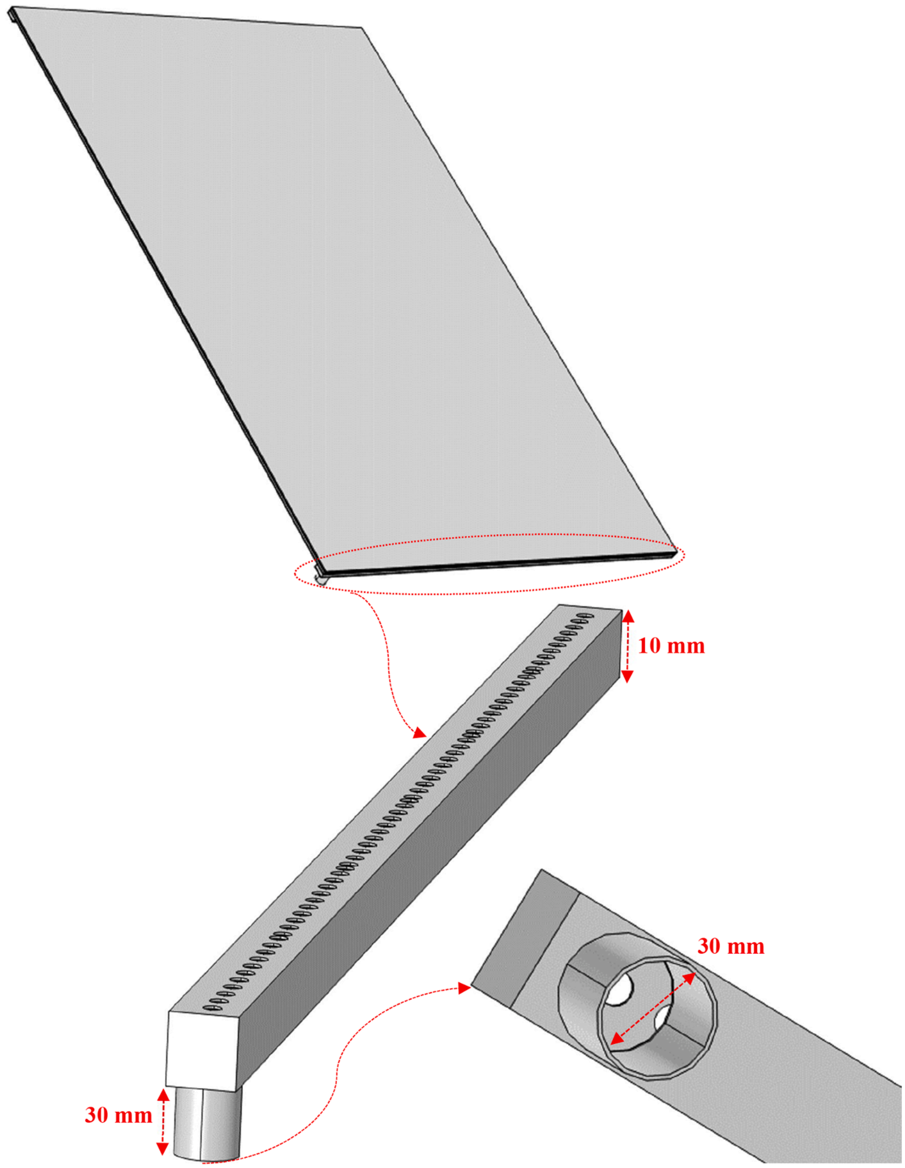

Fig. 3. Diagram of coolant distribution through HE inlet and outlet manifolds.

convective HT coefficient is 7.14 $W/m^2.K$, while a higher value of 150.0 $W/m^2 \cdot K$ was used for internal surfaces of the PVT-S, according to the literature [45–47].

❖ For the top surface:
- Heat flux: $-k_g \frac{\partial T_g}{\partial z} = G$
- Diffusive reflection: $-n.q = \varepsilon_g \sigma \left(T_s^4 - T_g^4\right)$, where σ = 5,670367 × $10^{-8} Wm^{-2}K^{-4}$ is Stefan-Boltzmann's constant.
- Convective heat loss: $-n.q = h_{g-a}(T_a - T_g)$

❖ For the interfaces:
- $\left(\frac{\partial T_s}{\partial n}\right)_{fluid} = \frac{k_s}{k_w}\left(\frac{\partial T_s}{\partial n}\right)_{solid}$

❖ All solid boundaries of the fluid channels are subject to the no-slip condition:
- $u = w = v = 0$

❖ For the inlet and outlet:
- Inlet: $T = T_{in}, u = U_{in}, w = v = 0$
- Outlet: $P = 0$ (Pa)

❖ For the PVT-S' (BC1, BC2, BC3) remaining boundaries:
- $\left(\frac{\partial T_s}{\partial n}\right) = 0$

2.4. First law (energy) analysis

The energy study is based on the theory of thermodynamics' first law. The schematic representation of the energy flow for the PVT-S under study is shown in Fig. 6. The inlet energy is symbolized by the amount of solar radiation, with significant outlet electrical and thermal energy. This approach considers the PVT-S as a unified control volume, allowing the energy balance for this volume to be formulated as follows [48]:

$$\sum E_{in} = \sum E_{out} + \sum E_{loss} \quad (5)$$

Where E_{loss}, E_{out} and E_{in} represent the system's energy losses, output energy, and input energy, respectively.

The effective total solar radiation incident on the PVT-S is calculated as follows [49]:

$$E_{in} = G\tau_g p_c \alpha_c A \quad (6)$$

The electrical energy generated corresponds to the portion of energy

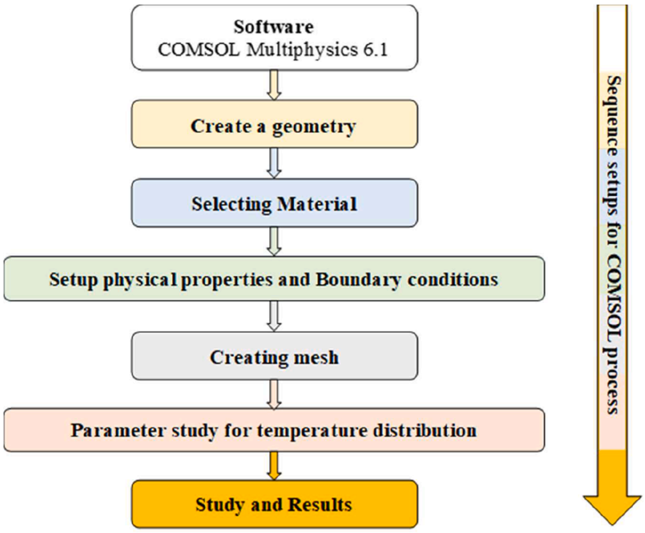

Fig. 4. Overall diagram used to simulate the PVT-S in COMSOL Multiphysics®.

absorbed by the PV cell, and is given by [50]:

$$E_p = \eta_c \tau_g \alpha_c G A p_c (1 - \mu_c (T_c - T_r)) \quad (7)$$

The PV cell temperature is determined using the equation presented below [51]:

$$T_c = \frac{P_c.G(\tau_g.\alpha_c - \eta_{ref}) + (U_{g-a} T_{amb} + U_t T_{ted})}{(U_{g-a} + U_t)} \quad (8)$$

The thermal energy recovered by the fluid from the PV module is calculated using the following equation [52]:

$$E_{th} = \dot{m} c_{p,f} (T_{out} - T_{in}) \quad (9)$$

This equation is used to evaluate the electrical performance of the PV panel:

$$\eta_{el} = \frac{E_p}{E_{in}} \quad (10)$$

The instantaneous PVT-S TE is determined using the equation presented below:

$$\eta_{th} = \frac{E_{th}}{E_{in}} \quad (11)$$

The equation below can be used to determine the overall PVT-S efficiency:

$$\eta_g = \frac{E_{th} + E_p}{E_{in}} \quad (12)$$

2.5. Second law (exergy) analysis

The methodology used in the exergy analysis is comparable to that used in the energy analysis. In this respect, Fig. 7 illustrates the exergy flow diagram of the PVT-S studied. The exergy approach is founded on the second law of thermodynamics principles. To assess the energy performance of the PVT-S, the first step is to consider it as a control volume.

The steady-state exergy balance of a PVT-S can be calculated as follows [53]:

$$\sum \dot{X}_{dest} = \sum \dot{X}_{in} - \sum \dot{X}_{out} \quad (13)$$

In this equation, $\dot{X}_{dest}$ represents the exergy destroyed as a result of irreversibility, $\dot{X}_{out}$ the output exergy, and $\dot{X}_{in}$ represents the input exergy.

The rate of exergy input, generally defined based on solar radiation, is calculated using the following expression [54]:

$$\dot{X}_{sun} = E_{in}\left[1 + \frac{1}{3}\left(\frac{T_{amb}}{T_{sun}}\right)^4 - \frac{4}{3}\left(\frac{T_{amb}}{T_{sun}}\right)\right] \quad (14)$$

Where T_{sun} denotes the black-body surface temperature of the sun, 5770 K [54].

The output exergy rate of the PVT-S, comprising thermal and electrical components, is given by the following expression [55]:

$$\sum \dot{X}_{th} + \sum \dot{X}_{el} = \sum \dot{X}_{out} \quad (15)$$

The thermal exergy (TEX),$\dot{X}_{th}$, is determined as follows:

$$\dot{X}_{th} = \dot{m} c_{p,f} (T_{out} - T_{in}) \times \left(1 - \frac{T_{amb}}{T_{out}}\right) \quad (16)$$

The calculation of the electrical exergy (EEX) is given by:

$$\dot{X}_{el} = \eta_{el} \times E_{in} \times \left[1 + \frac{1}{3}\left(\frac{T_{amb}}{T_{sun}}\right)^4 - \frac{4}{3}\left(\frac{T_{amb}}{T_{sun}}\right)\right] \quad (17)$$

TEX efficiency,ε_{th}, and EEX efficiency,ε_{el}, derived from the second law of thermodynamics, are defined as follows:

Table 2
Geometric, environmental, and thermophysical data used in modelling [39].

Parameter type	Description	Values
Collector geometry	Collector dimensions (L × W)	1.960 m × 0.960 m
Environmental conditions	Reference temperature (T_r)	25 °C
	Ambient temperature (T_{amb})	25 °C, 27 °C
	Solar irradiance (G)	$2 \times 10^2 - 10^3$ W/m²
Fluid inlet conditions	Inlet temperature (T_{in})	26 - 35 °C
	Inlet volume flow	30 - 180 L/h
PV properties	PV efficiency (at STC conditions) (η_{ref})	13%
	Solar cell packing factor (P_c)	0.95
	Solar cell absorptivity (α_c)	0.9
Glazing specifications	Glass emissivity (ε_g)	0.04
	Glass transmissivity (τ_g)	96%
Thermal parameters	PVT surfaces' HT coefficient (U_t)	150 $Wm^{-2}K^{-1}$
	Solar cell thermal efficiency coefficient (μ_c)	−0.0045%/ °C
	HT coefficient of glass-air (U_{g-a})	7.14 $Wm^{-2}K^{-1}$

Table 1
Hybrid PVT-S layers' properties [36].

Layer	Materials	Thickness (mm)	Thermal Conductivity [W/ (m. K)]	Heat capacitance C_p [J/(kg.K)]	Density ρ[Kg/m³]
HE	Aluminum		237	900	2700
	Copper	0.4	401	384	8960
Top cover	Glass	3	1.8	500	2500
Encapsulant	EVA	0.3	0.311	2090	950
Solar cell	Silicon	0.5	148	700	2329
Water	Fluid	-	0.68	4200	998
Bottom cover	Tedlar	0.1	0.15	1250	1200

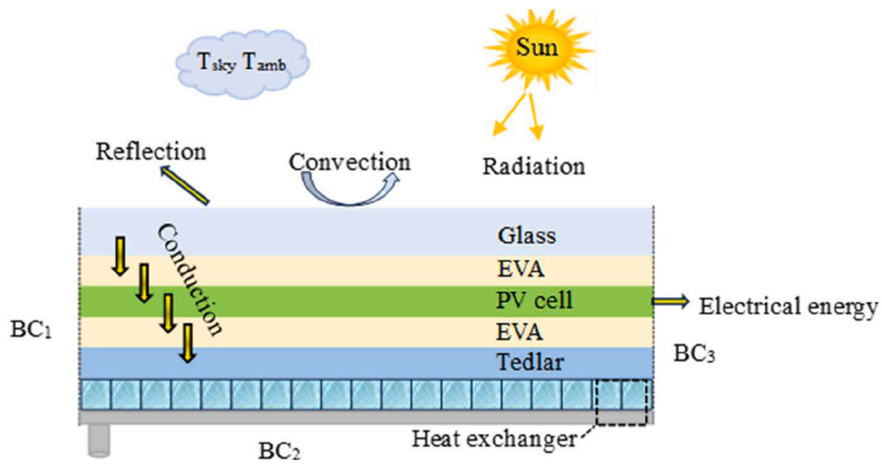

Fig. 5. Boundary conditions applied in the PVT-S simulation model.

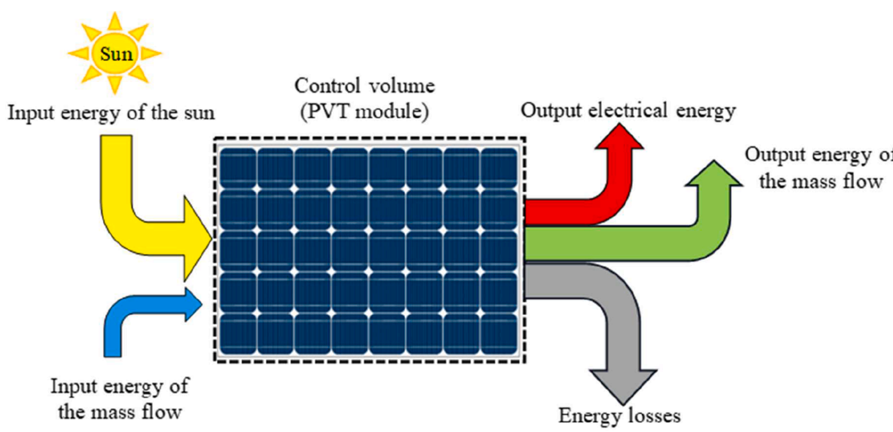

Fig. 6. Energy flow diagram for a PVT-S.

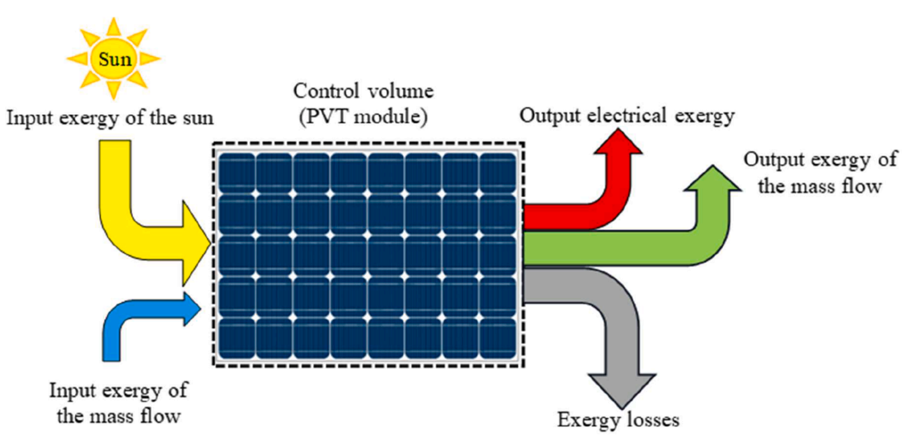

Fig. 7. Exergy flow diagram for PVT-S.

$$\varepsilon_{th} = \frac{\dot{X}_{th}}{\dot{X}_{in}} \times 100 \quad (18)$$

$$\varepsilon_{el} = \frac{\dot{X}_{el}}{\dot{X}_{in}} \times 100 \quad (19)$$

The overall exergy efficiency, $\varepsilon_{overall}$, is expressed by the following equation:

$$\varepsilon_{overall} = \frac{\dot{X}_{el} + \dot{X}_{th}}{\dot{X}_{sun}} = \varepsilon_{el} + \varepsilon_{th} \quad (20)$$

2.6. Mesh choosing

The development of the numerical model begins with the definition of boundary conditions, which is a prerequisite for generating the mesh needed to solve the discretized equations. In this study, the mesh for the

PVT-S was generated in COMSOL Multiphysics® using an automatic, physics-controlled meshing approach. A mesh sensitivity analysis was carried out to ensure that the simulation results are independent of the number of elements used. This verification was performed under the following operating conditions: an ambient temperature of 25 °C, and a fluid FR of 180 L/h. Several mesh densities were tested (Fig. 8), using the PV cell temperature as the main performance indicator. Among the configurations assessed, the one comprising 5791,537 elements proved sufficient: beyond this level, temperature variations between successive meshes became negligible. Since further refinement resulted in minimal accuracy improvement and significantly higher computational cost, this mesh configuration was selected for the simulations. Fig. 9 presents the 3D view of the uniform mesh structure used for the PVT-S.

2.7. Model confirmation

The numerical model was compared with experimental data published by Rahman et al. [56], who studied a SY-90 M PV module (1200 × 545) with strictly defined dimensions, connected to a copper HE consisting of seven tubes. This is a comparison of the temperature of the cells studied under three FRs (60, 90, and 180 L/h). In order to verify the evaluation, identical experimental conditions were reproduced in our simulation: radiation of 995 W/m^2, a fluid inlet temperature of 35 °C, and an ambient temperature of 27 °C. Table 3 presents the results of this comparison. The maximum deviation obtained is 4.39%, which proves the high accuracy of the developed model. The differences observed can be explained by a number of factors, such as the type of PV technology used in the reference study, the type of HE configuration used, and the rapid dynamics of environmental conditions, which are difficult to reproduce perfectly in a digital environment. Overall, by comparing the simulated results with the experimental results, we can say that the level of correspondence is high, which explains why the modeling methodology adopted is robust and reliable.

3. Results and discussion

To assess the performance of the new PVT-S system in terms of energy and exergy, this analysis has been conducted. Volumetric FRs (30–180 L/h), input temperature (26–35 °C), and solar irradiation levels (200–1000 W/m^2) were varied, and the T_{amb} was maintained at a temperature between 25 °C and 27 °C throughout the study. The subsequent sections present a comprehensive overview of the results obtained for each scenario analyzed.

3.1. Choice of material for the system developed

The optimum choice of PVT-S material is based on its ability to transfer heat efficiently [57]. It is important to seek high HT coefficients to ensure better thermal reduction in PVT-Ss. It is therefore essential to find an appropriate balance between the HT characteristics of the absorbent material and those of the fluid used. Materials frequently used in PVT-Ss include copper, aluminum, stainless steel, and polymers [58]. However, the use of stainless steel in the manufacture of PVT-Ss has major disadvantages, such as its weight and its propensity to corrode in environments with a pH above 7 [58]. Despite steel's good thermal conductivity and high convective HT coefficient, it is often considered unsuitable because of its incompatibility with various fluids and its manufacturing constraints.

Polymer materials have both advantages and disadvantages. A significant limitation is their lower thermal conductivity compared to copper and aluminum, which can result in boundary problems among thermal-PV components. Additionally, polymers tend to expand significantly with heat and are not well-suited to withstand the high temperatures present in PVT-S. Consequently, polymers are not recommended for designing and manufacturing heat absorbers in PVT-Ss. The choice of copper and aluminum as absorbent materials has been widely adopted by many researchers for the design of PVT-Ss [59]. This study evaluates the performance of a PVT-S using copper and aluminum as manufacturing materials to determine the more suitable option. Fig. 10(a) shows that the T_c in the aluminum PVT-S is slightly higher than in the copper PVT-S, with a maximum difference of 0.355 °C. This can be attributed to the thermal conductivity of the materials, as copper's higher conductivity allows for more efficient HT. Copper's superior heat dissipation allows the solar cell to operate at a slightly lower temperature than aluminum, resulting in a higher EE for the copper PVT-S, as shown in Fig. 10(b). However, the EE difference between the aluminum and copper PVT-Ss is only 0.174%, indicating comparable performance. Thus, due to its lower cost and lighter weight, aluminum is a viable material for thermal collectors in PVT-S applications.

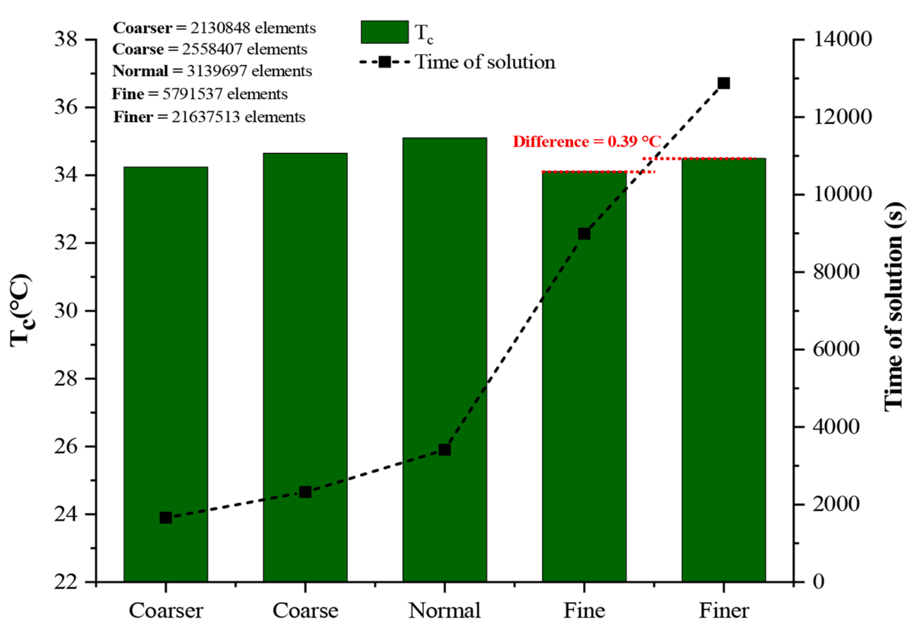

Fig. 8. Influence of mesh size on cell temperature.

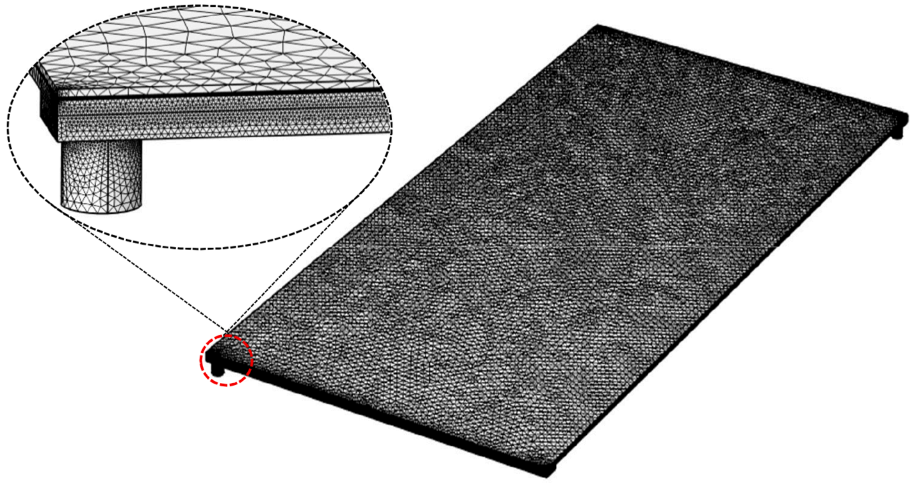

Fig. 9. PVT-S mesh.

Table 3
Validation of the cell temperature T_c model as a function of volume FR.

Flow rate (L/h)	T_c (°C)		Error (%)
	Present study	Rahman et al. [56]	
60	52.44	50.23	4.39%
90	49.54	49.65	0.22%
180	46.11	47.76	3.45%

3.2. Investigating the effect of irradiation

Streamline trajectories for the PVT-S were analyzed at irradiation levels of 2×10^2 to 10^3 W/m^2, with an FR of 180 L/h. Fig. 11 illustrates a case at 10^3 W/m^2, highlighting notable variations in the fluid's temperature distribution. Fig. 12 shows an in-depth analysis of the streamlines within the HE, focusing on two key points in the system. These streamlines allow the movement of the coolant through the HE to be visualized, and the corresponding temperatures can be determined by reference to the temperature bar provided in the figure. The average temperature of the water leaving the HE is directly related to solar irradiation levels. As solar radiation increases, the surface temperature of the PV panel rises, leading to greater heat production by the solar cells. This heat is absorbed by the Tedlar layer at the back of the PV panel, which enhances HT to the circulating cooling fluid in the HE. Thus, the fluid's average temperature at the outlet of the HE increases.

Fig. 13 shows how solar irradiation affects the PV panel temperature and the water outlet temperature for different water inlet temperatures (29 °C, 32 °C, and 35 °C). It can be seen that, whatever the inlet temperature, an increase in solar irradiation from 2×10^2 to 10^3 W/m^2 causes a simultaneous rise in the PV panel temperature (Fig. 13a) and the water outlet temperature (Fig. 13a). This is explained by the HT mechanism of the PVT-S. The temperature of the solar cell is proportional to solar irradiance, as shown in Eq. (8). As irradiance increases, the PV cell absorbs more heat, raising its temperature. This increased heat is transferred to the water circulating in the system, increasing the outlet temperature of the water. For a water input temperature of 29 °C, the PV panel temperature increases from 34.40 to 40.07 °C for the irradiance range (200 - 10^3 W/m^2). Similarly, water outlet temperature increases from 30.04 to 34.78 °C. For a water input temperature of 32 °C, the PV panel and water outlet temperatures increase respectively from 37.32 to 43.07 °C and from 32.68 to 37.40 °C with the irradiance range (200 - 10^3 W/m^2). Finally, at 35 °C fluid input temperature, the PV panel and fluid outlet temperatures increase from 40.15 to 46.03 °C and from 35.41 to 40.10 °C, respectively, for an irradiance range (200 - 10^3 W/m^2).

Fig. 14(a) shows that the EE decreases both with increasing solar irradiation and with increasing cooling water inlet temperature, whether at 29 °C, 32 °C, or 35 °C. PV cells absorb more photons when solar radiation increases, generating both more electrical current and more heat. The accumulated thermal energy raises the temperature of the cell, which increases the recombination of charge carriers and decreases the voltage across the cell terminals. This increase in electrical losses logically explains the decrease in EE under high irradiance, even though the total radiation flux is higher. In addition, a higher water inlet temperature reduces the ability of the cooling fluid to remove heat from the panel, thus reducing the efficiency of HT. For input temperatures of 29 °C, 32 °C and 35 °C, the efficiency decreases from 12.45% to 12.11%, from 12.27% to 11.94%, and from 12.11% to 11.76% respectively as the irradiance increases from 2×10^2 to 10^3 W/m^2, representing a decrease of 0.34%, 0.33% and 0.35% respectively.

Fig. 14(b) shows that TE increases as a function of solar irradiation for all three input temperatures (29 °C, 32 °C, and 35 °C). Furthermore, the TE increases as the input temperature decreases. For example, at 29 °C inflow temperature, the TE increases from 70.70% to 78.59% for escalating irradiance range (200 - 10^3 W/m^2). For input temperatures of 32 °C and 35 °C, the TE changes from 46.23% to 73.42% and from 27.87% to 69.34% respectively, again in response to a variation in irradiance from 2×10^2 to 10^3 W/m^2. In comparison, for 29 °C inflow temperature, a gain in TE of 9.25% is recorded compared with a 35 °C inflow temperature. The increase in irradiance increases the amount of heat generated by the PV cells. This additional heat spreads by conduction through the different layers of the panel to the HE, then is transferred to the heat transfer fluid by convection. Thus, as solar radiation increases, the heat flow to the fluid becomes greater, resulting in an increase in the TE of the PVT-S.

OE increases with irradiance, as shown in Fig. 14(c), due to the combined effect on electrical and thermal performance. Increased irradiance raises the temperature of the cells, which slightly reduces EE. However, this same temperature increase increases the amount of energy recovered by the fluid, thereby improving TE. The positive effect on TE compensates for the slight decrease in EE, leading to a net increase in the OE of the PVT-S. However, as noted above, the increase in TE predominates. OE rises from 83.15% to 90.7% for an input temperature of 29 °C. At 32 °C and 35 °C inflow temperatures, it rises from 58.5% to 85.36% and from 39.98% to 81.1% respectively, for irradiance range (200–10^3 W/m^2).

3.3. Investigation of the effect of volume flow rate

In this section of the study, we examine the effect of water FR on

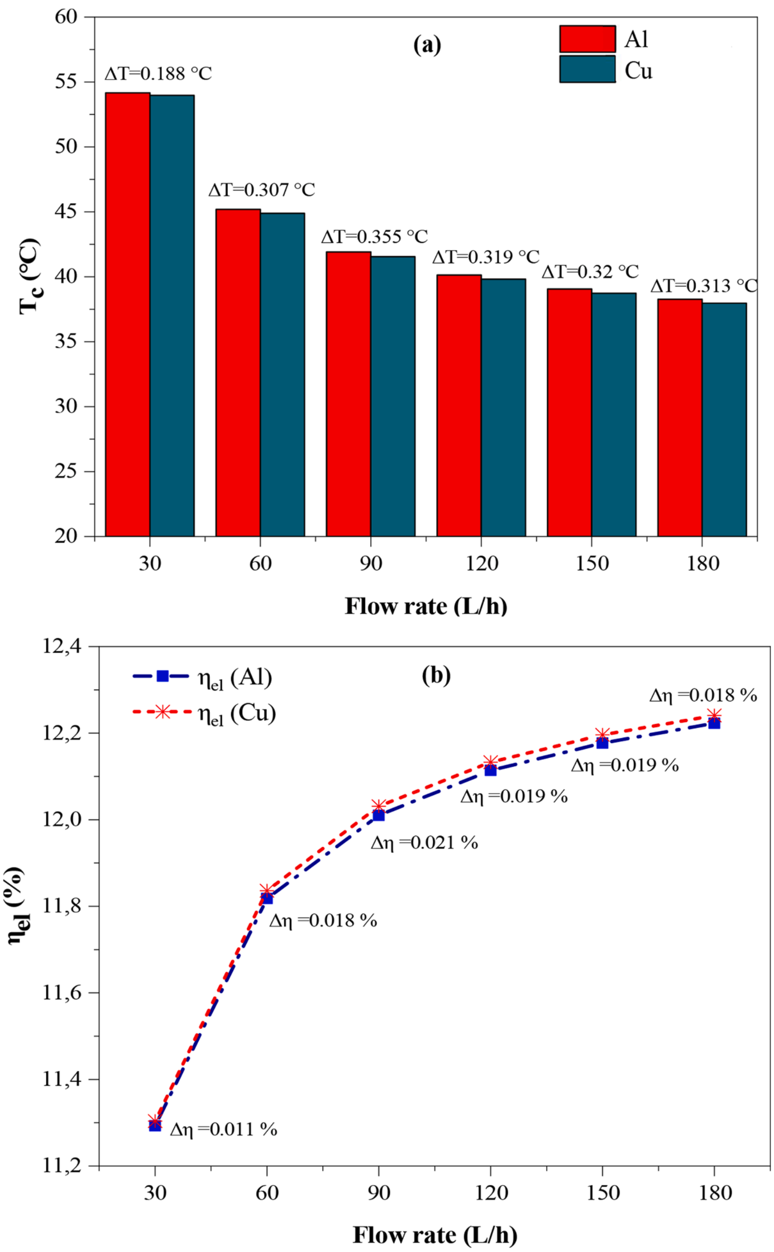

Fig. 10. Influence of water FR on (a) cell temperature and (b) EE of aluminum and copper PVT-Ss (Tin = 27 °C, Tamb = 27 °C, G = 10^3 W/m²).

Fig. 11. Water streamlines for T_{in} and G are 26 °C and 10^3 W/m^2, respectively.

PVT-S performance parameters. The range of variation of the inlet water FR was defined between 30 L/h and 180 L/h, with an interval of 30 L/h. These variations were studied at a constant input temperature of 26 °C, under irradiation of 10^3 W/m^2.

Fig. 15 shows that increasing the FR reduces the PV panel and outflow temperatures. The PV panel reaches a peak temperature of 53.07 °C at a 30 L/h FR. However, it drops to 37.05 °C at a 180 L/h FR. This reduction is mainly due to improved convective HT: a higher FR increases fluid velocity, which improves HT between the PV panel surface and the cooling fluid. However, this increase in fluid velocity reduces the time the fluid spends in contact with the panel, which reduces its ability to accumulate heat. As a result, the fluid outlet temperature also drops, from 49.34 °C with a low FR of 30 L/h to 31.95 °C with a high FR of 180 L/h.

Fig. 16(a) shows that increasing the water FR from 30 L/h to 180 L/h results in a significant improvement in the TE and EE of the PVT-S. With a higher FR, the water circulates more quickly through the system, allowing more efficient extraction of heat from the PV panel. This increased heat extraction increases the TE of the system, as more heat is transferred to the water. At the same time, the increase in water flow results in a decrease in the average temperature of the PV cells. Although

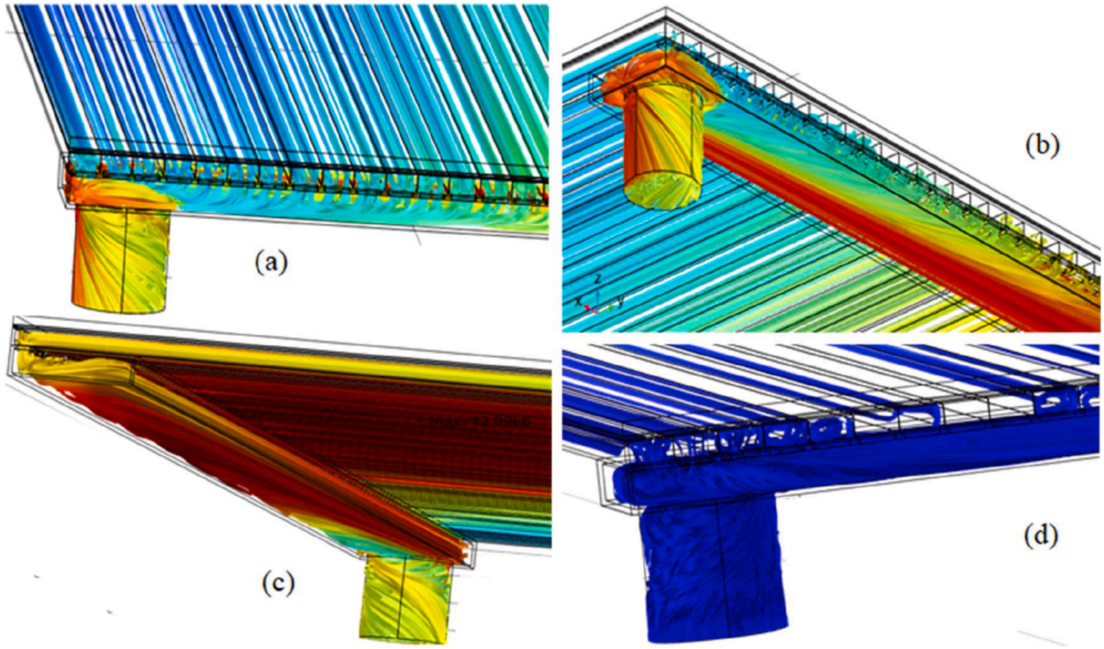

Fig. 12. Exploded view of the streamlines at the input (d) and output (a-c) of the HE.

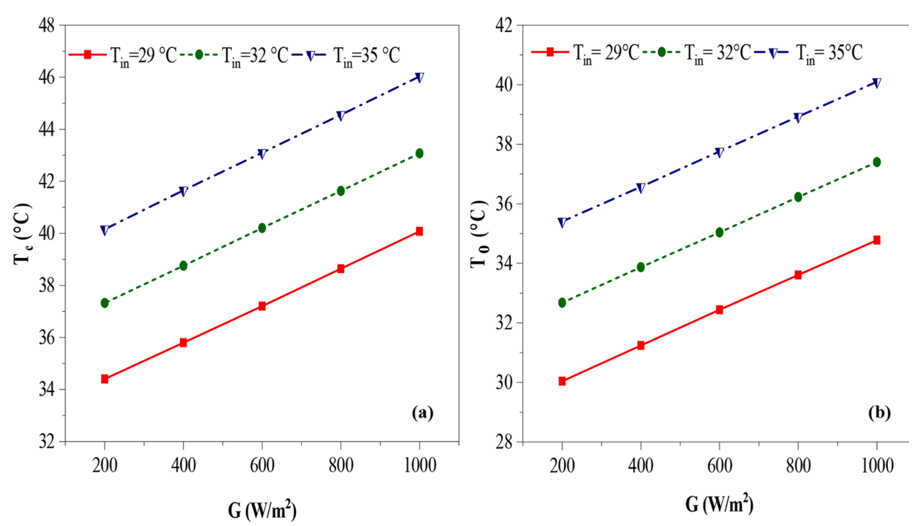

Fig. 13. Evolution of (a) PV panel temperature and (b) water outlet temperature as a function of irradiance for different input temperature values (29 °C, 32 °C, and 35 °C).

the PVT-S current may decrease slightly, the voltage generated by the system increases significantly. This increase in voltage leads to an increase in the EE and power output of the system, despite the slight decrease in current. The OE increases as the thermal and electrical efficiencies increase with the fluid inlet FR, as shown in Fig. 16(b). For example, at a low FR of 30 L/h, the electrical, thermal, and overall efficiencies are 11.35%, 52.89% and 64.24% respectively. However, at a higher FR of 180 L/h, the thermal, electrical, and overall efficiencies are 12.29%, 80.90% and 93.19% respectively.

3.4. *Investigation of the effect of input water temperature*

Fig. 17 shows the temperature distributions of the PVT-S for four different inlet temperatures, set between 26 °C and 35 °C, with a FR and irradiance of 80 L/h and 10^3 W/m^2. Whatever the inlet temperature, the panel temperature remains relatively low near the fluid inlet, where the cold water initially absorbs heat. Moving away from the inlet towards the outlet, the panel temperature gradually increases, due to the heating of the water as it passes through. The top left of the panel, identified as the hottest zone, is where the water reaches its maximum temperature before exiting the system. This area is subject to greater thermal build-up due to prolonged exposure to irradiance and the heat generated by the PV conversion process.

Fig. 18 demonstrates the evolution of PV cell temperature T_c and EE in relation to the input water temperature. It is clear that the heat removal capacity of the water decreases as the inlet fluid temperature increases. In other words, more thermal energy is transferred to the PV cells, causing the PV cell temperature to rise from 31.95 °C to 40.10 °C. As a result, at higher water input temperatures, the water fails to cool the PV panel effectively, resulting in a decrease in its EE from 12.29% to 11.76%, a reduction of 0.53%.

As shown in Fig. 19, as the input temperature increases, the

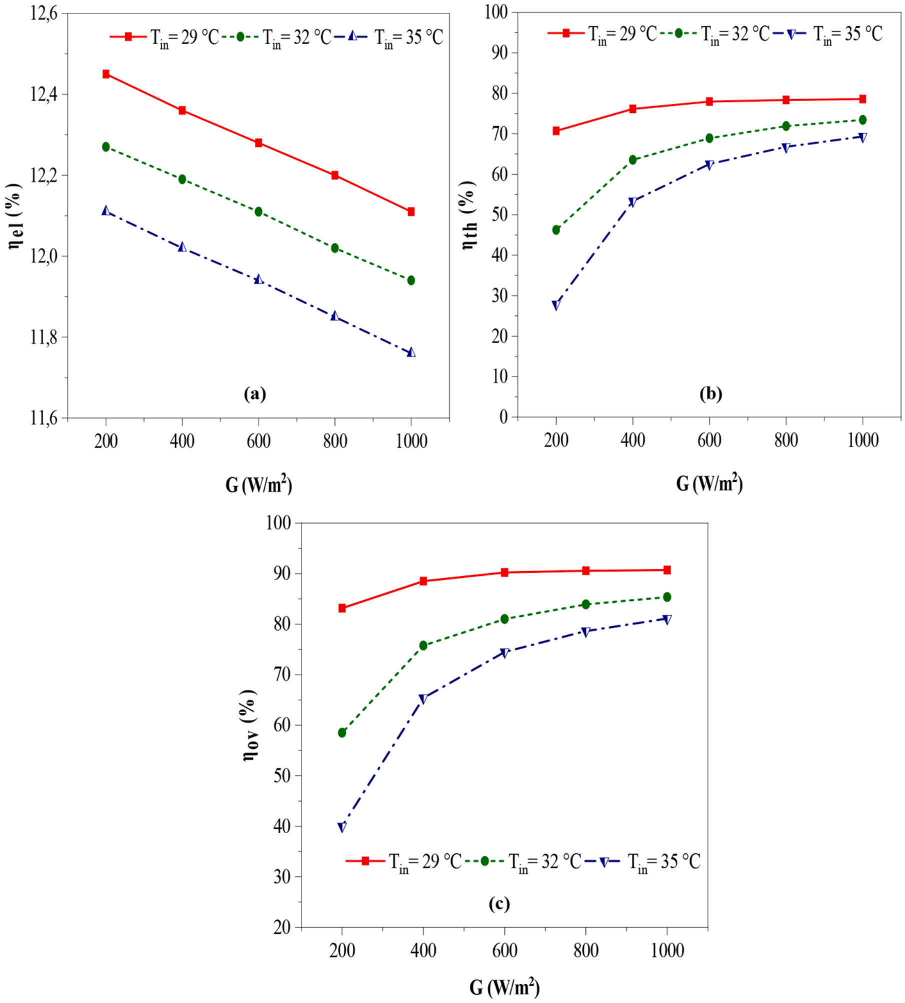

Fig. 14. Variation in (a) EE, (b) TE, and (c) OE as a function of solar radiation for different input temperatures (29 °C, 32 °C, and 35 °C).

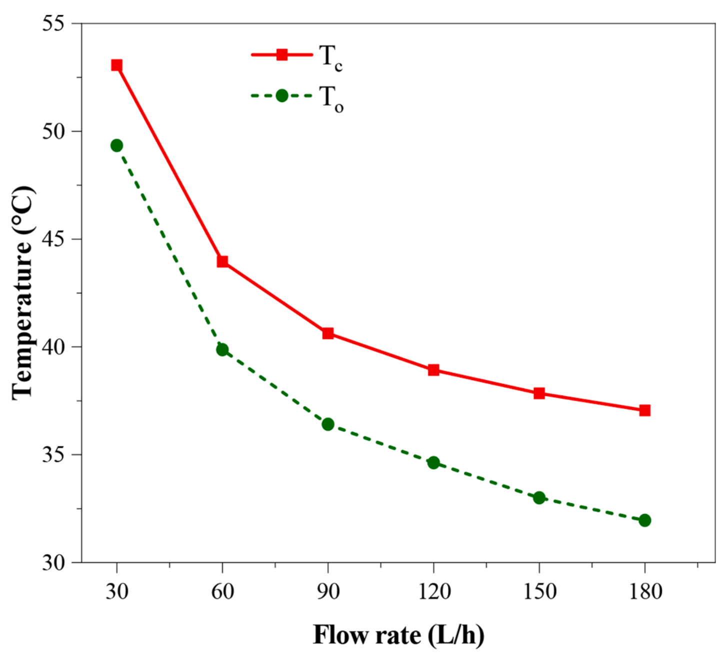

Fig. 15. Variation in outlet and PV temperature against FR.

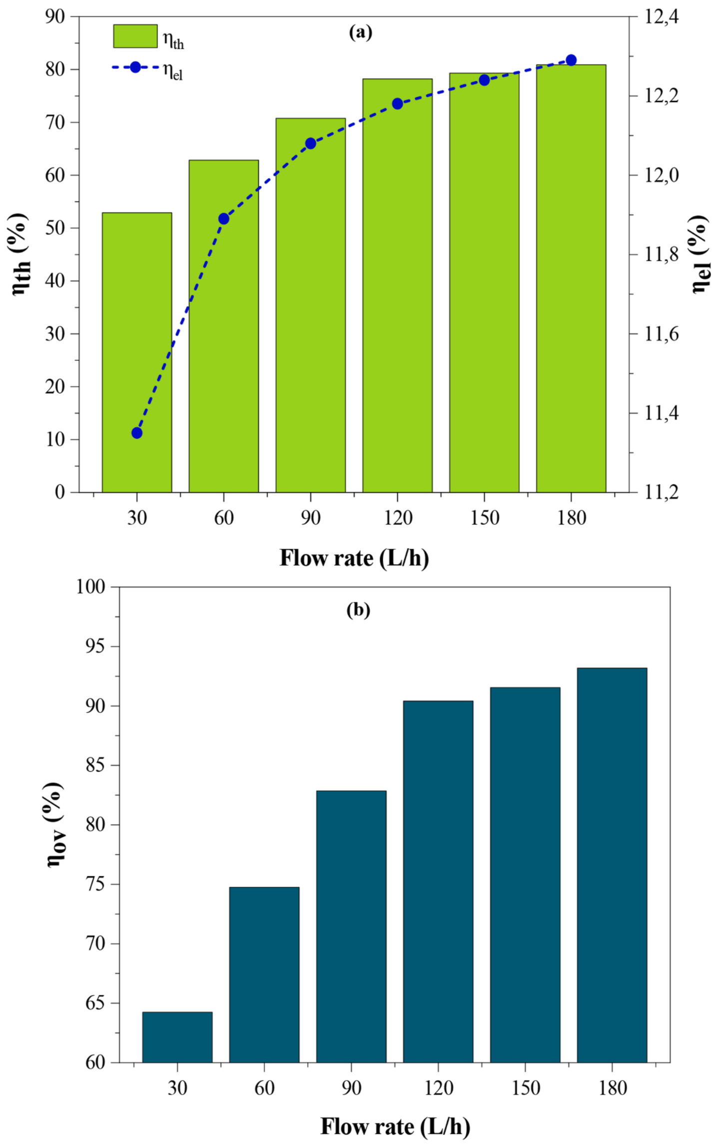

Fig. 16. Variation of (a) EE and TE and (b) OE as a function of FR.

temperature difference between the inlet and outlet gradually decreases. Specifically, it decreases from approximately 5.95 °C at an input temperature of 26 °C to only 5.1 °C when the inlet water is heated to 35 °C. This decrease is mainly due to excessive heat loss to the environment. Consequently, the convective HT rate decreases, ultimately leading to a reduction in the TE of the PVT-S from 80.90% to 69.34%. Another factor contributing to this reduction in TE is the decrease in the heat transport capacity of the water, observed as the input water temperature increases.

3.5. Exergy analysis for the PVT system

This section focuses on evaluating the exergy performance of the PVT-S examined in this research in order to measure its actual operating efficiency. A notable limitation of the first law of thermodynamics is that it neglects energy quality and focuses on all forms of energy, such as electrical, mechanical, chemical, and thermal energy, which can lead to inaccurate assessments by ignoring the nuances specific to each form of energy [60]. To obtain a more qualitative assessment of the PVT-S's performance, an analysis based on the second law of thermodynamics is performed, taking into account the irreversibility associated with thermal processes. The exergy analysis is performed using Eqs. (13) to (20) and explicitly defining the reference environment at an ambient temperature of 25 °C, in accordance with the methodology used in this article and proposed by Kalogirou et al.[54]., which ensures the reproducibility of the results and the clarity of the approach. This approach highlights the differences between energy performance and exergy performance. Energy optimization aims to maximize the total amount of heat or electricity recovered, while exergy optimization detects and reduces losses due to irreversibility and improves the quality of the energy extracted. Although this study did not perform a detailed analysis by component, global modeling allows total losses to be estimated and the main trends in the system to be identified. This approach provides solid guidance for the design and management of PVT-S, and can serve as a basis for future studies aimed at analyzing irreversibility in each component in greater detail. In practical terms, this distinction is important because it translates performance gains into concrete and measurable benefits such as reduced pump consumption, lower thermal stresses, and increased electricity production. Analysis based on the first law of thermodynamics alone shows superior performance due to the neglect of losses and the qualitative omission of energy values.

The variations in EEX and TEX of the PVT-S as a function of increasing volumetric FR from 30 L/h to 180 L/h, at a constant inlet temperature of 26 °C and solar irradiance of 10^3 W/m^2, are presented in

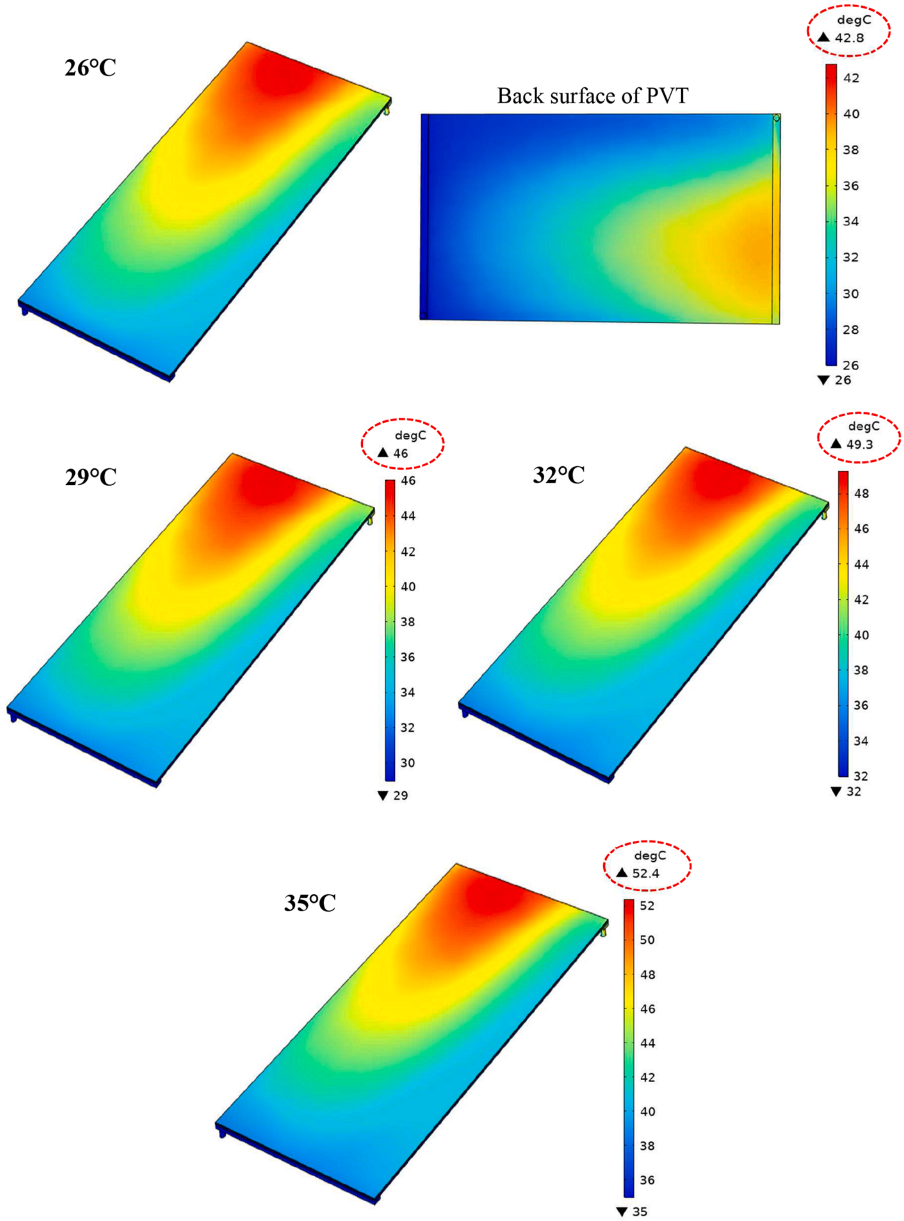

Fig. 17. PVT-S temperature distribution for different input temperatures.

Fig. 20(a). It is observed that increasing the FR leads to a decrease in TEX and an increase in EEX. Specifically, TEX decreases by 51.82%, while EEX increases by 7.62% as the FR rises. This opposite trend can be explained by the reduction in fluid residence time within the collector at higher FRs, which limits heat absorption and reduces the outlet fluid temperature, thereby decreasing the TEX. Conversely, the increase in FR enhances the cooling of PV cells, lowering their operating temperature and improving EE, which leads to a rise in EEX. Due to the more significant reduction in TEX compared to the increase in EEX, the total exergy efficiency decreases by approximately 8.18% (Fig. 20(b)). The overall exergy efficiency of the PVT-S reaches its maximum (15.63%) at a flow rate of 30 L/h and its minimum (14.35%) at 180 L/h. The main sources of exergy destruction are identified as thermal irreversibilities due to temperature gradients in the PV cells and the working fluid, as well as mechanical irreversibilities related to friction and fluid flow. Increasing the FR raises fluid velocity, which not only intensifies these internal irreversibilities but also increases pumping power requirements and pressure losses. Consequently, the exergy destruction rate grows with increasing FR, highlighting the trade-offs that must be considered for system design and optimization, such as balancing thermal, electrical, and pumping performance to achieve maximum OE.

At an inlet temperature of 29 °C and a FR of 180 L/h, the results show that increasing solar irradiance enhances both thermal and electrical energy production, leading to higher TEX and EEX outputs (Fig. 21(a)). As solar irradiance increases from 200 to 1000 W/m^2, TEX rises from 3.63 to 38.55 W, while EEX increases from 35.80 to 174.14 W. This simultaneous increase is mainly attributed to the higher incident solar energy, which raises both the heat absorbed by the working fluid and the electrical power generated by the PV cells. Moreover, higher irradiance intensifies the temperature difference between the system and the ambient, thereby increasing the exergy potential of the thermal output. This significant enhancement in both thermal and electrical exergy leads to an increase in the total exergy efficiency of approximately 7.30% (Fig. 21(b)). The maximum total exergy efficiency of the PVT-S reaches 14.79% at the highest irradiance level (1000 W/m^2), while the minimum value of 13.71% is recorded at 200 W/m^2. This trend indicates that the exergy gain due to increased useful energy output outweighs the associated thermal losses at higher irradiance levels, resulting in an

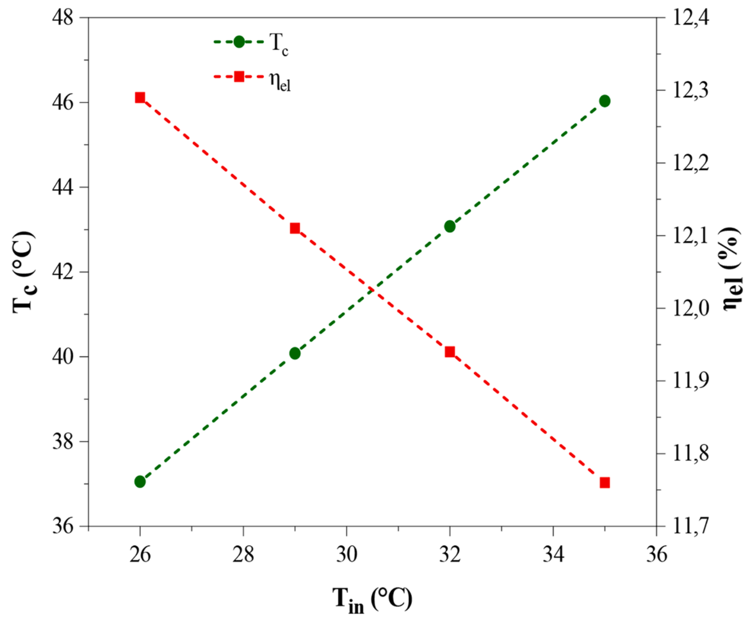

Fig. 18. Evolution of PV temperature and EE as a function of input water temperature.

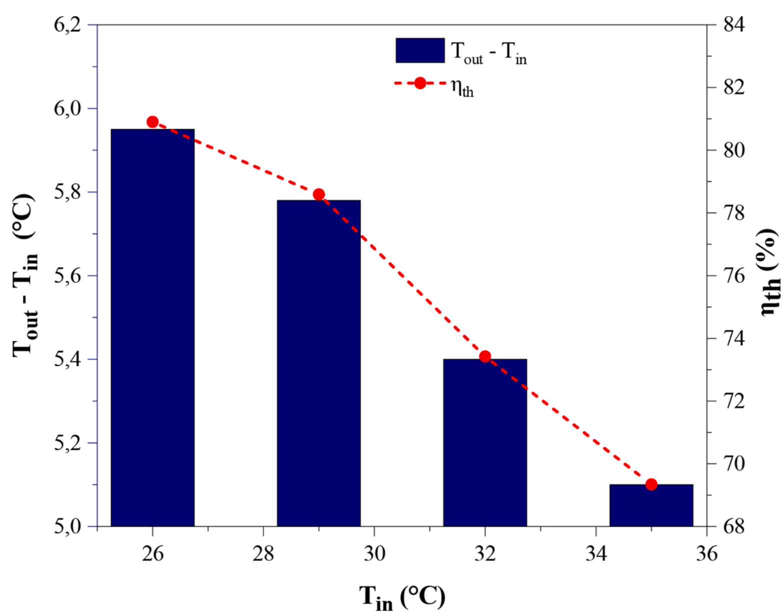

Fig. 19. The temperature difference between output and input water, as well as TE, varies with the temperature of the input water.

overall improvement in system performance.

Fig. 22(a) illustrates the influence of water inlet temperature on the electrical and thermal exergy efficiencies (EEX and TEX) of the PVT-S system, with the FR fixed at 180 L/h under an irradiance of 10^3 W/m^2. It can be observed that when the inlet temperature increases from 26 °C to 35 °C, TEX increases by 44.86%, whereas EEX decreases by 4.31%. This opposite behavior can be explained by the thermal gradient between the PV cells and the coolant: a higher inlet temperature reduces the temperature difference, leading to a lower cooling effect on the PV cells and thus a slight reduction in EE. As the inlet temperature increases, TEX efficiency improves significantly (Fig. 22(b)), reaching a maximum of 3.59%. This enhancement is mainly due to the increase in the mean fluid temperature, which raises the exergy content of the extracted thermal energy, since exergy is strongly dependent on temperature level relative to ambient conditions. However, the EEX efficiency reaches its maximum value of 12.29% at the lowest inlet temperature of 26 °C. At lower inlet temperatures, the cooling of PV cells is more effective, reducing cell temperature and consequently improving electrical conversion efficiency. Furthermore, the maximum total exergy efficiency of 15.35% is achieved at an inlet temperature of 35 °C. This indicates that, despite the slight drop in electrical performance, the gain in TEX dominates the overall system behavior at higher inlet temperatures. Thus, from a second-law analysis perspective, the PVT-S system examined in this study reaches optimal overall performance at an FR of 30 L/h and an inlet temperature of 35 °C.

3.6. *Investigation of pressure*

Fig. 23 displays the exchanger channels' pressure distribution under 1000 W/m^2 irradiation and an FR of 180 L/h. The higher-pressure

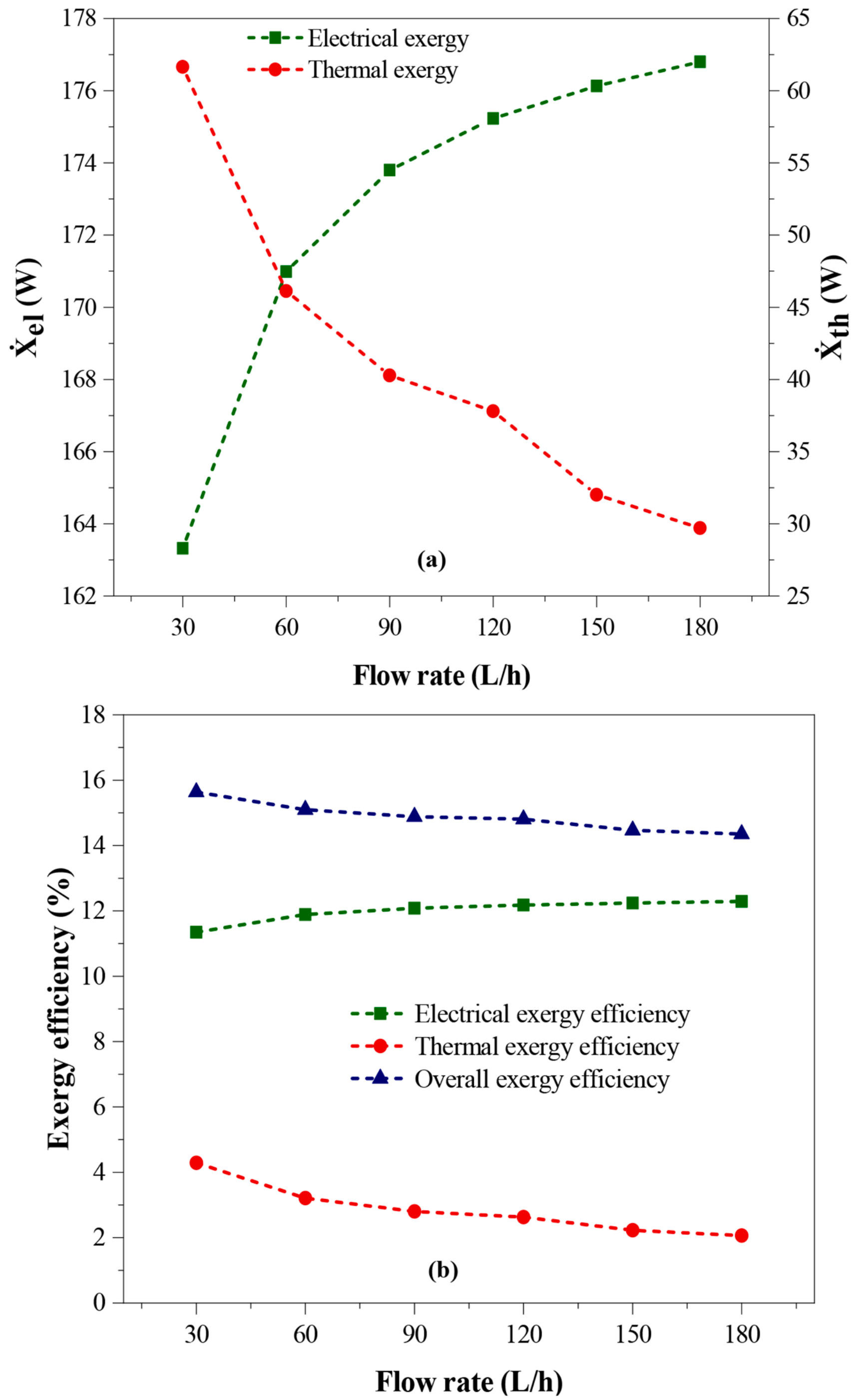

Fig. 20. Variation of (a) TEX and EEX, and (b) exergy performance as a function of FR.

region appears at the inlet because of the increased velocity of the cooling fluid. This high pressure results from the initial stress exerted by the narrow channels on the incoming fluid. Moving away from the inlet, the pressure gradually decreases along the channels, a decrease that is due to friction between the fluid and the channel walls, as well as the loss of kinetic energy of the fluid as it moves. This pressure distribution, typical of forced-flow systems, shows a steady reduction in pressure towards the outlet, reflecting the balance between frictional head losses and energy dissipation within the system.

Fig. 24 shows the pressure drop in a channel positioned directly at the exchanger inlet, with increasing FRs maintained at a constant G of 10^3 W/m². The figure clearly indicates that as the FR increases from 30 to 180 L/h, the pressure drop from the exchanger inlet to the outlet rises significantly, reflecting the higher pumping requirements associated with increased FRs. For an FR of 30 L/h, the pressure varies between 5.27 Pa at the exchanger inlet and 0.22 Pa at the outlet. At an FR of 120 L/h, the pressure changes from 49.04 Pa at the inlet to 0.8 Pa at the outlet. At the highest FR of 180 L/h, the pressure drop further increases, ranging from 97.10 Pa at the exchanger input to 1.1 Pa at the outlet. These results highlight that higher volumetric FRs, while potentially enhancing thermal and electrical performance, also substantially increase the energy required for pumping, emphasizing the trade-off between system efficiency and operational energy consumption.

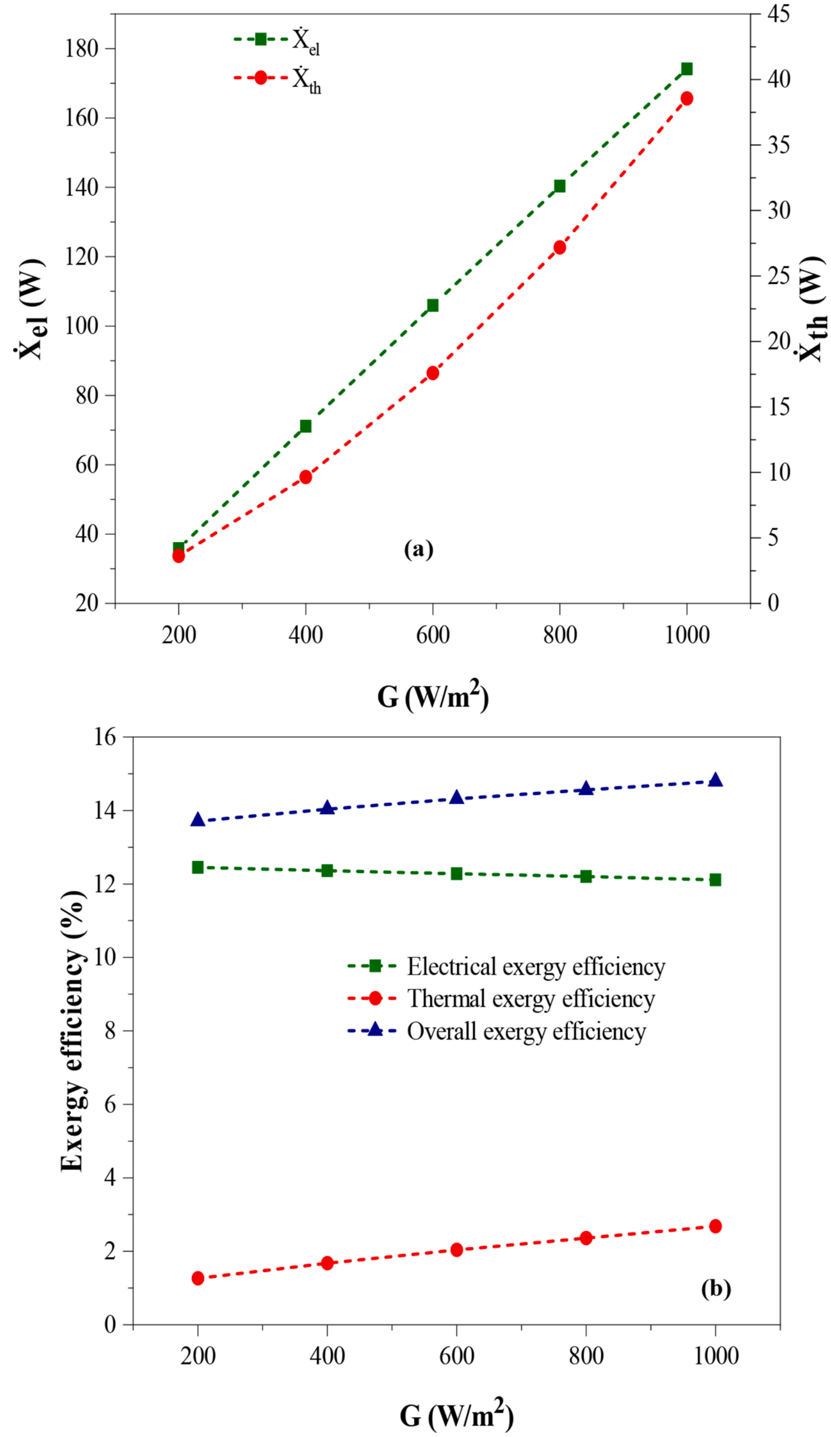

Fig. 21. Variation of (a) TEX and EEX, and (b) exergy performance as a function of irradiance.

3.7. Comparison with the literature

3.7.1. Cell temperature

Table 4 illustrates the average change in PV cell temperature (T_c) for a 100 W/m² upsurge of solar irradiance, based on various published studies. Reported values range from 0.9 °C to 2.7 °C, reflecting the diversity of technologies and cooling methods. In our study, the average temperature increase per increment of irradiance is lower, at around 0.7 °C, confirming the system's more efficient thermal management. This superior performance can be explained by the specific geometry of the channel-shaped HE, which increases the contact surface between the heat transfer fluid and the wall while ensuring a more uniform flow distribution. Thanks to this configuration, the thermal resistance between the module layers and the fluid is reduced, allowing for faster and more uniform heat extraction compared to conventional structures. This feature is the key innovation in our design and explains the observed decrease in panel temperature despite the increase in irradiance. Thus, the low temperature rise measured not only demonstrates better control of overheating, but also distinguishes our system as a more thermally efficient solution than conventional cooling systems [39,49,65–67].

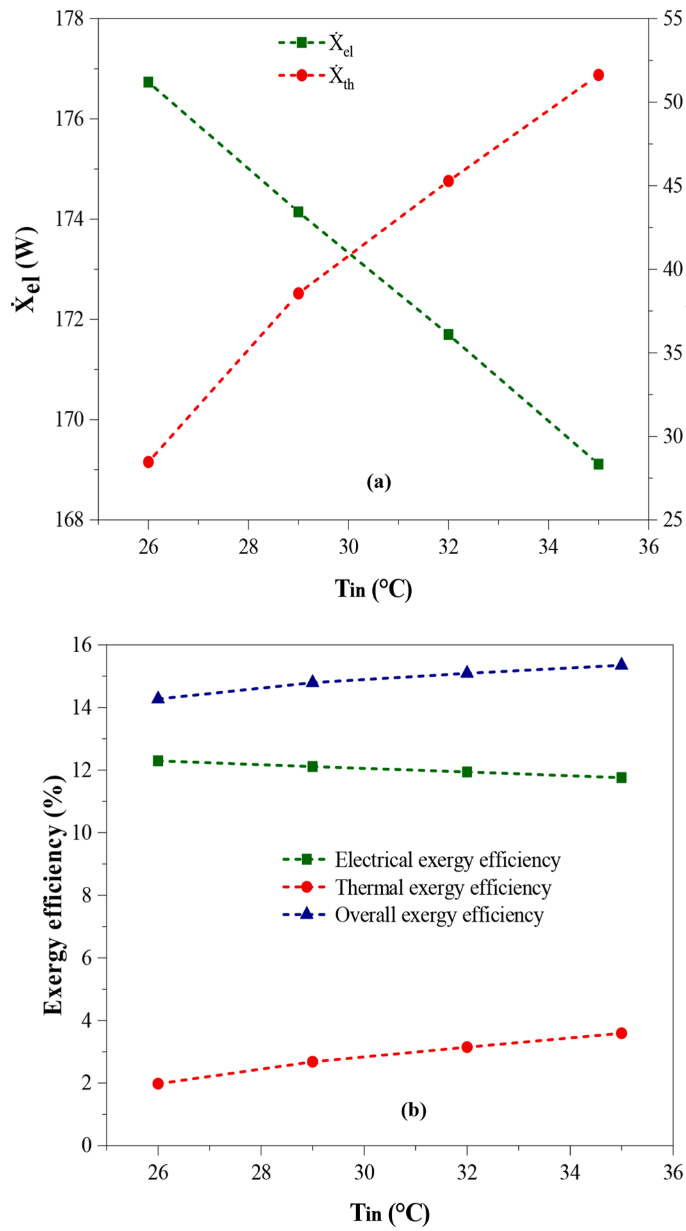

Fig. 22. Variation of (a) TEX and EEX, and (b) exergy performance as a function of water inlet temperature.

3.7.2. *Thermal efficiency*

A comparative analysis was conducted by comparing the results of this study with those of other relevant studies using numerical simulations with COMSOL software [66,67]. Fig. 25 presents the conclusions of this comparison, showing that the TE obtained in this study reaches a remarkably high level of 80.90% for an FR of 180 L/h and an inlet temperature of 26 °C, whereas the values reported in previous studies range between 72% and 76%. This comparison validates the performance of the system under study and confirms that the proposed cooling device is more effective at maintaining lower cell temperatures compared to existing configurations.

3.7.3. *Regression equation*

At a FR of 180 L/h and an input temperature T_{in} of 35 °C, a linear equation is deduced for the solar cell temperature and EE of the PVT-S using regression analysis. The value of the confidence coefficient in this numerical regression equation is $R^2 = 0.9998$. The traditional simple linear expression for PV panel efficiency is given by Eq. (10). The comparison of the linear regression equations between the present numerical analysis and that of Nasrin et al. [46], who used a PVT-S with a box channel, is shown in Table 5. For a solar cell temperature T_c of 25 °C, the calculated difference between the current numerical results and those of Nasrin et al. [46] is only 0.15%. Consequently, there is good agreement between these two results.

3.7.4. *Correlation*

Numerical simulations established that the irradiance was correlated with cell temperature. This relation was determined under moderate irradiance conditions (200–1000 W/m²), with coolant FR and inflow temperature of 180 L/h and 29 °C, respectively. The corresponding expression is given below:

$$T_c = 20.18 \times G^{0.0928} \text{where} R^2 = 97.6\%.$$

We compared it with those derived from numerical and experimental methods as presented by [64]. Table 6 shows that the three correlations for solar cell temperature at 600 W/m² irradiation have a percentage error of <2%. This small error can be attributed to factors like PV size, irradiation range, fill factor, operating conditions, materials properties,

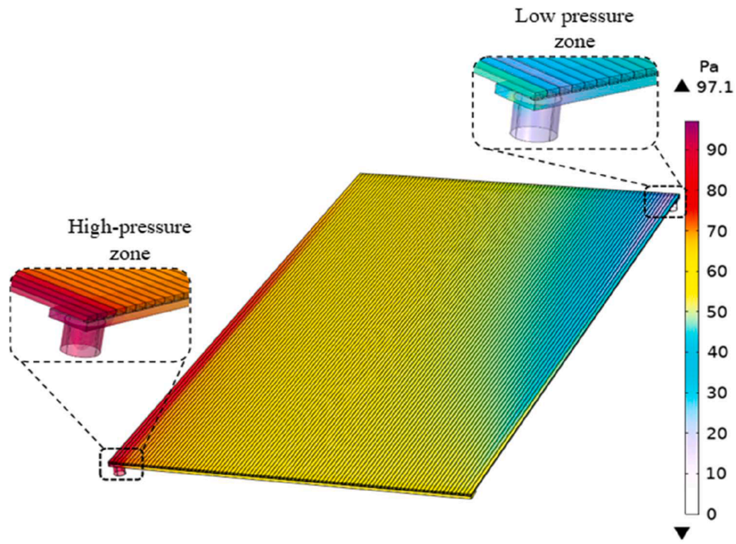

Fig. 23. Exchanger channels' pressure delivery at irradiance and FR of 10^3 W/m^2 and 180 L/h, respectively.

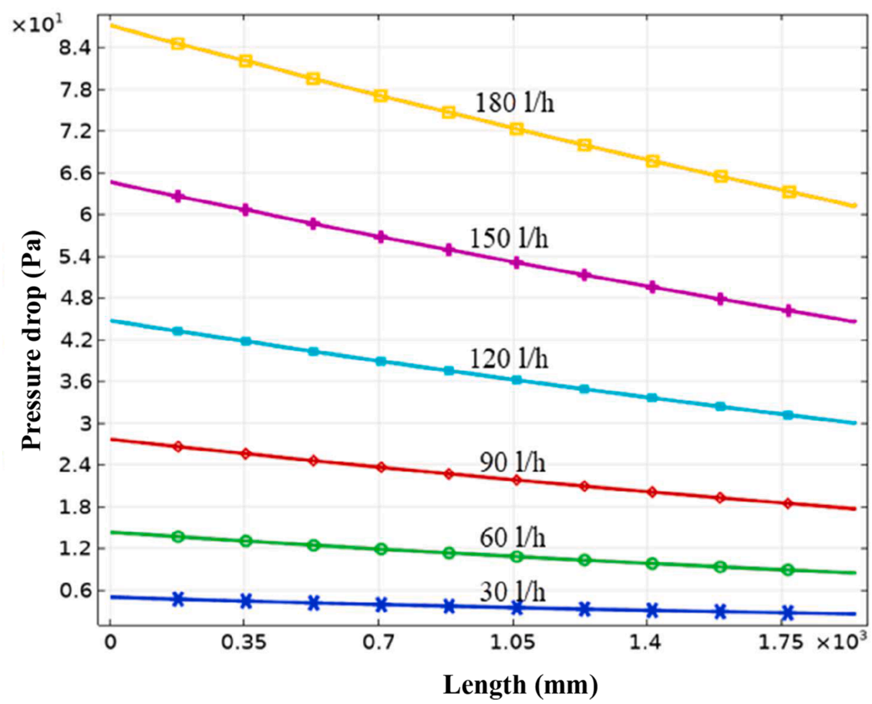

Fig. 24. Pressure drop in a channel positioned at the exchanger inlet, with increasing volume FRs from 30 to 180 L/h, under constant G of 10^3 W/m^2.

reference and water input temperatures.

4. Study limitations

Before finalizing this study, it is important to acknowledge certain factors that may limit the interpretation of the results. The numerical model developed is based on idealized conditions that do not always reflect the operational reality of a PVT-S. For example, the presence of dust or deposits on the surface of the PV module, frequently observed in the field, was not taken into account, even though it can influence OE. In addition, the thermal and physical properties of the materials were considered to be invariant, which reduces the complexity of the calculation but does not reflect potential variations related to temperature changes. Certain external parameters, such as humidity or wind fluctuations, were not included in the modeling, even though they can have a significant impact on the behavior of the system. It should also be noted that the actual environmental conditions observed during the experimental tests are difficult to reproduce identically in a simulation setting. This natural difference between the real and virtual environments may explain some of the discrepancies observed between the numerical and experimental validation results.

5. Conclusions

This study proposes and investigates a new channel-box HE integrated directly into a PV module, consisting of 94 channels to form a novel PVT-S system. The objective is to evaluate the energy and exergy performance of the system under different operating conditions, considering the effects of solar irradiance, inlet fluid temperature, and volumetric FR. Three-dimensional modeling was performed using

Table 4
Evaluation of solar cell temperature (T_c) in this study compared to existing literature.

References	Cooling channel shape	T_{amb} (°C)	G (W/m²)		T_c (°C) increment per 100 W/m² irradiance
			Starting	Ending	
Bahaidarah et al. [61]	Cooling panel	21	240	979	1.9
Nasrin et al. [46]	A box-shaped channel	32	1000	3000	1.85
Shen et al. [62]	Shark dorsal fin type channel	20	300	1200	1.29
Rahman et al. [56]	Baffles in the channel	35	312	995	2.71
Chandrasekar et al. [63]	Cotton wick structures	37	600	1300	1.4
Nasrin et al. [64]	Baffle structures	32	1000	5000	0.9
Teo et al. [65]	A parallel array of finned ducts	-	550	1050	1.4
Present research	channel-shaped HE	25	200	1000	0.7

COMSOL Multiphysics with the FEM, and the results were validated against experimental data and literature. The main conclusions are summarized below:

- Validation of the numerical model showed a good agreement between the numerical and experimental results for temperature and EE of the PVT-S, with errors of <5%.
- The results demonstrate that the PVT-S with an aluminum HE performs very similarly to a copper exchanger, with an EE difference of just 0.174% and a maximum solar cell temperature variation of 0.355 °C. Since aluminum is lighter and less expensive than copper, it can be considered a viable alternative for the heat collector material in PVT-S.
- The increase in solar radiation resulted in an increase in all efficiency values, with the exception of EE. By way of illustration, at an input temperature of 29 °C, OE increased by 7.55%, TE rose by 7.89%, while EE fell by 0.34%. In addition, this increase in solar radiation had a positive impact on overall exergy efficiency, resulting in an increase of around 7.30%.
- Increasing the FR had beneficial effects on the parameters of the first PVT-S law. By way of illustration, an increase in FR from 30 L/h to

Table 6
Comparative analysis between the regression equation formulated in this study and that developed by [64], both experimentally and numerically.

References	Research	Irradiation (W/m²)	Correlation	T_c (°C) at 600 W/m²	Error (%)
Nasrin et al. [64]	Experimental	300–1000	$T_c = 2.9692 \times G^{0.3948}$	37.10	1.53
Nasrin et al. [64]	Numerical using COMSOL	1000–5000	$T_c = 3.4913 \times G^{0.3641}$	35.85	1.91
Present research	Numerical using COMSOL	200–1000	$T_c = 20.18 \times G^{0.0928}$	36.53	

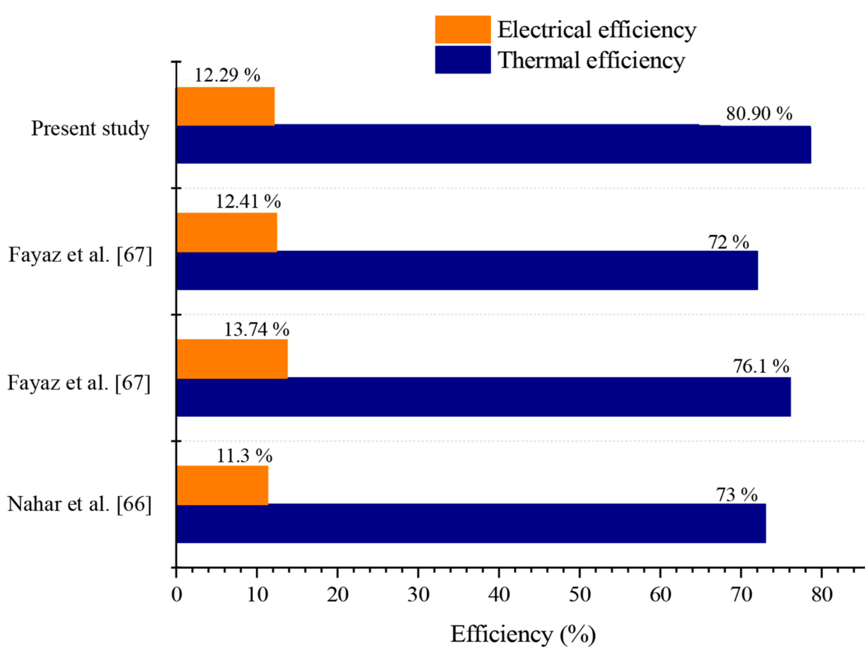

Fig. 25. Comparison of efficiencies with other relevant numerical studies, using COMSOL software.

Table 5
Comparison between the equation obtained in this study and that developed by [46].

References	G (W/m²)		T_c (°C)		Equation	Efficiency at T_c= 25 °C	Error (%)
	Starting	Ending	Starting	Ending			
Nasrin et al. [46]	1000	3000	48	85	$\eta = 0{,}151 - 0.00088 \times T_c$	12.9	0.15
Present research	200	1000	34.40	40.07	$\eta = 0{,}144 - 0.00059 \times T_c$	12.92	

180 L/h, at an inlet temperature of 29 °C, resulted in a 0.94%, 28.01% and 28.95% improvement in electrical, thermal, and overall efficiencies, respectively. On the other hand, contrary to what was observed with the first law, increasing the FR had an unfavorable impact on the parameters of the second law. At 26 °C inflow temperature and 1000 W/m^2 irradiance, the PVT-S achieves a maximum exergy efficiency of 15.63% and it drops to 14.35% at a FR of 30 L/h and 180 L/h, respectively.
- Increasing inlet temperature reduces the water's cooling capacity, lowering both EE and TE. For 180 L/h and 1000 W/m^2, EE drops by 0.53% and TE by 11.56%. Higher temperatures improve thermal and total exergy efficiency but decrease EEX. The PVT-S achieves optimal overall performance at 30 L/h and 35 °C inlet temperature.

6. Future work

In future work, several areas of research deserve further exploration in order to broaden the practical and economic implications of this study. One avenue is to explore the use of metal matrix composites as an alternative to conventional metallic materials for the design of tubes and absorbers. These materials could offer better thermal conductivity, greater durability, and reduced weight, which could potentially help lower the manufacturing and maintenance costs of PVT-Ss. It would also be useful to conduct an in-depth analysis of the impact of the thermal gradient between cooled and uncooled areas on the durability of PV modules in order to better estimate the actual lifespan of the system. A more precise understanding of this aspect would allow for the integration of advanced economic models, particularly in terms of reducing costs associated with premature aging and increasing the operating life of the panels. Furthermore, the improved performance observed in this study will need to be translated into concrete economic indicators such as the cost of energy produced (LCOE), potential annual savings, reduced return on investment time, and the financial impact for different user sectors (residential buildings, industrial facilities, greenhouse agriculture, etc.). These analyses will enable a more accurate quantification of the economic benefits associated with the adoption of the PVT-S. Finally, an essential step will be to experimentally validate this new PVT-S in order to confirm its actual performance, refine the associated economic models, and assess its feasibility on a large scale in a variety of applications.

Funding declaration

This research received no specific grant from any funding agency in the public, commercial, or not-for-profit sectors.

CRediT authorship contribution statement

Yassine El Alami: Writing – original draft, Visualization, Validation, Software, Methodology, Investigation, Formal analysis, Data curation, Conceptualization. **Mohamed El Habib Amagour:** Writing – review & editing, Validation, Supervision, Funding acquisition, Data curation. **Rehena Nasrin:** Writing – review & editing, Validation, Methodology, Investigation. **Fatima Majid:** Writing – review & editing, Software, Resources, Investigation, Data curation. **Redouane Rmaily:** Writing – review & editing, Resources, Investigation, Formal analysis, Data curation. **Elhadi Baghaz:** Writing – review & editing, Methodology, Investigation, Data curation, Conceptualization. **Khaled M. Al-Aribe:** Writing – review & editing, Investigation, Funding acquisition, Formal analysis, Data curation, Conceptualization. **Adnan Ibrahim:** Writing – review & editing, Project administration, Investigation, Formal analysis, Data curation, Conceptualization.

Declaration of competing interest

The authors declare that they have no known competing financial interests or personal relationships that could have appeared to influence the work reported in this paper.

Data availability

The datasets generated and/or analysed during the current study are available from the corresponding author, upon reasonable request.

References

[1] S.S. Ibrahim, H. Hamzah, A. Alkhabbaz, A. Albojamal, K. Vafai, Thermal management of the PV-PCM module via arc-porous fins, Therm. Sci. Eng. Prog. 71 (2026) 104533, https://doi.org/10.1016/j.tsep.2026.104533.
[2] M. Khatibi, R. Nemati-Farouji, A. Taheri, A. Kazemian, T. Ma, H. Niazmand, Optimization and performance investigation of the solidification behavior of nano-enhanced phase change materials in triplex-tube and shell-and-tube energy storage units, J. Energy Storage 33 (2021) 102055, https://doi.org/10.1016/j.est.2020.102055.
[3] A. Taheri, M. Malayjerdi, M. Kazemi, H. Kalani, R. Nemati-Farouji, M. Passandideh-Fard, M. Sardarabadi, Improving the performance of a nanofluid-based photovoltaic thermal module utilizing dual-axis solar tracker system: experimental examination and thermodynamic analysis, Appl. Therm. Eng. 196 (2021) 117178, https://doi.org/10.1016/j.applthermaleng.2021.117178.
[4] S. Jamal, A. Alkhabbaz, H. Hamzah, B. Sahin, Thermal analysis of a solar panel unit using PCM and various fin arrangements, Int. J. Heat Fluid Flow 117 (2026) 110108, https://doi.org/10.1016/j.ijheatfluidflow.2025.110108.
[5] Y. El Alami, M. Rami, C. Hajjaj, M. Benhmida, A. Faize, E. Baghaz, Three-dimensional thermal modeling and analysis of the heat source, the impact of encapsulation materials and the back sheet of silicon PV modules, Appl. Therm. Eng. 280 (2025) 128430, https://doi.org/10.1016/j.applthermaleng.2025.128430.
[6] Y.E. Alami, E. Baghaz, R. Nasrin, C. Hajjaj, M. Benhmida, K.M. Al-Aribe, A. Ibrahim, Numerical exploration and relational impact ranking of critical parameters in 3D PV module studies, Results Eng (2025) 107097, https://doi.org/10.1016/j.rineng.2025.107097.
[7] Y.E. Alami, B. Zohal, R. Bendaoud, M. Rhiat, A. Rabhi, B. Benhala, K. Hirech, E. Baghaz, Comparative analysis of the performance of Shingle and Standard photovoltaic technologies in the environmental conditions of El Jadida, in: E3S Web Conf 601, 2025 00010, https://doi.org/10.1051/e3sconf/202560100010.
[8] Y. El Alami, E. Chetouani, H. Mokhliss, F. Ouerradi, M. Aoutoul, S. Bounouar, R. Bendaoud, A. Faize, R. Rmaily, Optimizing solar energy efficiency with an improved hill-climbing maximum power point tracking control approach: hardware implementation, Clean Energy 8 (2024) 167–176, https://doi.org/10.1093/ce/zkae061.
[9] Y. El Alami, E. Baghaz, R. Nasrin, M. Al-Damook, R. Bendaoud, T. Bouragba, M. Melhaoui, M. Benhmida, Up-to-date review on flat-plate solar hybrid photovoltaic Thermal systems: absorber designs and fabrication materials, Int. J. Energy Res. 2025 (2025) 5547555, https://doi.org/10.1155/er/5547555.
[10] M. Hissouf, M. Feddaoui, M. Najim, A. Charef, Numerical study of a covered photovoltaic-Thermal collector (PVT) enhancement using nanofluids, Sol. Energy 199 (2020) 115–127, https://doi.org/10.1016/j.solener.2020.01.083.
[11] A.A.A. Anazi, M.I. Alghamdi, A. Chammam, M.S. Kadhm, I.H. Al-Kharsan, R. Alayi, Theoretical analysis of an integrated, CPVT membrane distillation system for cooling, heating, power and seawater desalination, Water (Basel) 15 (2023) 1345, https://doi.org/10.3390/w15071345.
[12] M.C. Browne, B. Norton, S.J. McCormack, Heat retention of a photovoltaic/thermal collector with PCM, Sol. Energy 133 (2016) 533–548, https://doi.org/10.1016/j.solener.2016.04.024.
[13] T.T. Chow, A review on photovoltaic/thermal hybrid solar technology, Appl. Energy 87 (2010) 365–379, https://doi.org/10.1016/j.apenergy.2009.06.037.
[14] Y.E. Alami, E. Baghaz, R. Nasrin, K. Haboubi, M. Benhmida, A. Ibrahim, Integrated sustainability and 4E analysis of hybrid nanofluid featured PVT systems incorporating diverse backsheets, Appl. Therm. Eng. (2025) 129147, https://doi.org/10.1016/j.applthermaleng.2025.129147.
[15] A.S. Abdelrazik, F. Al-Sulaiman, R. Saidur, R. Ben-Mansour, A review on recent development for the design and packaging of hybrid photovoltaic/thermal (PV/T) solar systems, Renew. Sustain. Energy Rev. 95 (2018) 110–129, https://doi.org/10.1016/j.rser.2018.07.013.
[16] A.K. Azad, S. Parvin, T. Hossain, Performance evaluation of nanofluid-based photovoltaic thermal (PVT) system with regression analysis, Heliyon 10 (2024) e29252, https://doi.org/10.1016/j.heliyon.2024.e29252.
[17] L.W. Florschuetz, Extension of the Hottel-Whillier model to the analysis of combined photovoltaic/thermal flat plate collectors, Sol. Energy 22 (1979) 361–366, https://doi.org/10.1016/0038-092X(79)90190-7.
[18] A. Ibrahim, M.Y. Othman, M.H. Ruslan, M.A. Alghoul, M. Yahya, A. Zaharim, K. Sopian, Performance of photovoltaic thermal collector (PVT) with different absorbers design, WSEAS Trans. Environ. Dev. 5 (2009).
[19] M. Rafid, A.K. Azad, S.M. Prottoy, S. Alam, M. Rahman, Md.J. Miah, M.S. Hossain, M.M. Rahman, Augmentation of heat exchanger performance with hybrid nanofluids: identifying research gaps and future indications - A review, Int. Commun. Heat Mass Transf. 155 (2024) 107537, https://doi.org/10.1016/j.icheatmasstransfer.2024.107537.

[20] F. Hussain, M.Y.H. Othman, B. Yatim, H. Ruslan, K. Sopian, Z. Anuar, S. Khairuddin, An improved design of photovoltaic/thermal solar collector, Sol. Energy 122 (2015) 885–891, https://doi.org/10.1016/j.solener.2015.10.008.

[21] Y. El Alami, H. El Achouby, R. Nasrin, C. Hajjaj, M. Benhmida, E. Baghaz, M. Ghazal, A. Ibrahim, Numerical and experimental analysis of a new direct-contact PVT system for sustainable energy production: energy, exergy, and environmental assessments, Energy 348 (2026) 140542, https://doi.org/10.1016/j.energy.2026.140542.

[22] A.N. Özakin, F. Kaya, Effect on the exergy of the PVT system of fins added to an air-cooled channel: a study on temperature and air velocity with ANSYS Fluent, Sol. Energy 184 (2019) 561–569, https://doi.org/10.1016/j.solener.2019.03.100.

[23] M. Emam, A. Hamada, H.A. Refaey, M. Moawed, M.A. Abdelrahman, M.R. Rashed, Year-round experimental analysis of a water-based PVT-PCM hybrid system: comprehensive 4E assessments, Renew. Energy 226 (2024) 120354, https://doi.org/10.1016/j.renene.2024.120354.

[24] S. Misha, A.L. Abdullah, N. Tamaldin, M.A.M. Rosli, F.A. Sachit, Simulation CFD and experimental investigation of PVT water system under natural Malaysian weather conditions, Energy Rep 6 (2020) 28–44, https://doi.org/10.1016/j.egyr.2019.11.162.

[25] A. Nahar, M. Hasanuzzaman, N.A. Rahim, A three-dimensional comprehensive numerical investigation of different operating parameters on the performance of a photovoltaic thermal system with pancake collector, J. Sol. Energy Eng. 139 (2017) 031009, https://doi.org/10.1115/1.4035818.

[26] H.A. Refaey, S. Abdo, H. Saidani-Scott, Y.A. El-Shekeil, S. Bendoukha, N. Barhoumi, M.A. Abdelrahman, Thermal regulation of photovoltaic panels using PCM with multiple fins configuration: experimental study with analysis, Therm. Sci. Eng. Prog. 49 (2024) 102457, https://doi.org/10.1016/j.tsep.2024.102457.

[27] Y. Yu, H. Yang, J. Peng, E. Long, Performance comparisons of two flat-plate photovoltaic thermal collectors with different channel configurations, Energy 175 (2019) 300–308, https://doi.org/10.1016/j.energy.2019.03.054.

[28] A. Hamada, M. Emam, H.A. Refaey, M. Moawed, M.A. Abdelrahman, Investigating the performance of a water-based PVT system using encapsulated PCM balls: an experimental study, Energy 284 (2023) 128574, https://doi.org/10.1016/j.energy.2023.128574.

[29] D. De Luca, A. Caldarelli, E. Gaudino, E. Di Gennaro, M. Musto, R. Russo, Modeling of energy and exergy efficiencies in high vacuum flat plate photovoltaic–thermal (PV–T) collectors, Energy Rep 9 (2023) 1044–1055, https://doi.org/10.1016/j.egyr.2022.11.152.

[30] A.Z. Sheshpoli, O. Jahanian, K. Nikzadfar, M.A. Delavar, Numerical and experimental investigation on the performance of hybrid PV/thermal systems in the north of Iran, Sol. Energy 215 (2021) 108–120, https://doi.org/10.1016/j.solener.2020.12.036.

[31] Y. El Alami, E. Baghaz, M. Errebii, R. Nasrin, M.E.H. Amagour, K.M. Al-Aribe, A. Ibrahim, Numerical perspective of copper nanoparticle morphology on energy conversion in a novel photovoltaic-thermal system, Energy 342 (2026) 139598, https://doi.org/10.1016/j.energy.2025.139598.

[32] S. Mohammadi, F.R. Astaraei, Tube cross-section flatness optimization to enhance the cooling performance of nanofluid-based photovoltaic thermal systems combined with nano-enhanced phase change material, J. Energy Storage 99 (2024) 113343, https://doi.org/10.1016/j.est.2024.113343.

[33] M. Madadi, A.A. Abbasian Arani, Experimental evaluation of photovoltaic thermal (PVT) system using a modular heat collector with flat back shape fins, pipe, nanofluids and phase change material, Sol. Energy Mater. Sol. Cells 280 (2025) 113294, https://doi.org/10.1016/j.solmat.2024.113294.

[34] F.A. Radhi, A. Ibrahim, H.L. Azeez, A. Fazlizan, K. Sopian, A.A. Ali, A.B. Al-Aasam, Experimental analysis of a photovoltaic thermal collector utilizing a novel spring insert in a micro-fin absorber tube with twisted tape, nanofluid, and nanophase change material integration, Appl. Therm. Eng. 269 (2025) 126128, https://doi.org/10.1016/j.applthermaleng.2025.126128.

[35] A. Kazemian, K. Khosravi, S. Sen, P. Talebizadehsardari, A. Cairns, T. Ma, Optimizing photovoltaic thermal systems with wavy collector tube: a response surface-based design study with desirability analysis, Appl. Therm. Eng. 258 (2025) 124475, https://doi.org/10.1016/j.applthermaleng.2024.124475.

[36] Y.E. Alami, A. Lamkaddem, R. Bendaoud, S. Talbi, M. louzazni, E. Baghaz, Numerical study of a water-based photovoltaic-thermal (PVT) hybrid solar collector with a new heat exchanger, E-Prime Adv. Electr. Eng. Electron. Energy 9 (2024) 100693, https://doi.org/10.1016/j.prime.2024.100693.

[37] T.T. Chow, J. Ji, W. He, Photovoltaic-thermal collector system for domestic application, J. Sol. Energy Eng 129 (2006) 205–209, https://doi.org/10.1115/1.2711474.

[38] Y. El Alami, A. Ameur, M. Benhmida, A. Rabhi, E. Baghaz, Performance evaluation of different new channel box photovoltaic thermal systems, J. Clean. Prod. 478 (2024) 143953, https://doi.org/10.1016/j.jclepro.2024.143953.

[39] Y. El Alami, H.E. Achouby, E. Baghaz, C. Hajjaj, R. Nasrin, An innovative photovoltaic thermal system with direct water-cell contact: energy, exergy, and sustainability analysis, Sol. Energy 300 (2025) 113827, https://doi.org/10.1016/j.solener.2025.113827.

[40] A. Alqatamin, S. Jinzhan, Numerical analysis and design of photovoltaic-thermal (PVT) system with novel water-cooling channel structure integrated with perforated V-shape fins, Renew. Energy 243 (2025) 122587, https://doi.org/10.1016/j.renene.2025.122587.

[41] A. Alqatamin, J. Su, Computational analysis of photovoltaic thermal performance using Al2O3/water and CNT/water nanofluids with perforated V-shape heatsink, Energy 334 (2025) 137793, https://doi.org/10.1016/j.energy.2025.137793.

[42] A. Alqatamin, J. Su, Machine learning prediction of photovoltaic-thermal system with V-shaped perforated fins, Appl. Therm. Eng. 280 (2025) 128344, https://doi.org/10.1016/j.applthermaleng.2025.128344.

[43] H. Fayaz, N.A. Rahim, M. Hasanuzzaman, A. Rivai, R. Nasrin, Numerical and outdoor real time experimental investigation of performance of PCM based PVT system, Sol. Energy 179 (2019) 135–150, https://doi.org/10.1016/j.solener.2018.12.057.

[44] B. Zhao, H. Song, Fuzzy Shannon wavelet finite element methodology of coupled heat transfer analysis for clearance leakage flow of single screw compressor, Eng. Comput. 37 (2021) 2493–2503, https://doi.org/10.1007/s00366-020-01259-6.

[45] S. Dubey, A.A.O. Tay, Testing of two different types of photovoltaic–thermal (PVT) modules with heat flow pattern under tropical climatic conditions, Energy Sustain. Dev. 17 (2013) 1–12, https://doi.org/10.1016/j.esd.2012.09.001.

[46] R. Nasrin, M. Hasanuzzaman, N.A. Rahim, Effect of high irradiation on photovoltaic power and energy, Int. J. Energy Res. 42 (2018) 1115–1131, https://doi.org/10.1002/er.3907.

[47] Y. El Alami, E. Baghaz, R. Bendaoud, R. Nasrin, Pressure drops reduction and performance optimization strategies of an innovative channel box photovoltaic thermal system, Int. J. Photoenergy 2025 (2025) 8744508, https://doi.org/10.1155/ijph/8744508.

[48] M. Sardarabadi, M. Hosseinzadeh, A. Kazemian, M. Passandideh-Fard, Experimental investigation of the effects of using metal-oxides/water nanofluids on a photovoltaic thermal system (PVT) from energy and exergy viewpoints, Energy 138 (2017) 682–695, https://doi.org/10.1016/j.energy.2017.07.046.

[49] S. Alsaqoor, A. Alqatamin, A. Alahmer, Z. Nan, Y. Al-Husban, H. Jouhara, The impact of phase change material on photovoltaic thermal (PVT) systems: a numerical study, Int. J. Thermofluids 18 (2023) 100365, https://doi.org/10.1016/j.ijft.2023.100365.

[50] A.K. Azad, S. Parvin, Photovoltaic thermal (PV/T) performance analysis for different flow regimes: a comparative numerical study, Int. J. Thermofluids 18 (2023) 100319, https://doi.org/10.1016/j.ijft.2023.100319.

[51] A. Alqatamin, O.A. Al-Khashman, J. Su, A novel heatsink for optimizing photovoltaic cell performance with passive cooling using perforated wave-shaped fins, J. Sol. Energy Eng 147 (2025), https://doi.org/10.1115/1.4068410.

[52] B. Zhao, Y. Ren, D. Gao, L. Xu, Y. Zhang, Energy utilization efficiency evaluation model of refining unit based on Contourlet neural network optimized by improved grey optimization algorithm, Energy 185 (2019) 1032–1044, https://doi.org/10.1016/j.energy.2019.07.111.

[53] S. Abbas, J. Zhou, A. Hassan, Y. Yuan, S. Yousuf, Y. Sun, C. Zeng, Economic evaluation and annual performance analysis of a novel series-coupled PV/T and solar TC with solar direct expansion heat pump system: an experimental and numerical study, Renew. Energy 204 (2023) 400–420, https://doi.org/10.1016/j.renene.2023.01.032.

[54] S.A. Kalogirou, S. Karellas, K. Braimakis, C. Stanciu, V. Badescu, Exergy analysis of solar thermal collectors and processes, Prog. Energy Combust. Sci. 56 (2016) 106–137, https://doi.org/10.1016/j.pecs.2016.05.002.

[55] F. Yazdanifard, M. Ameri, Exergetic advancement of photovoltaic/thermal systems (PV/T): a review, Renew. Sust. Energy Rev. 97 (2018) 529–553, https://doi.org/10.1016/j.rser.2018.08.053.

[56] M.M. Rahman, M. Hasanuzzaman, N.A. Rahim, Effects of operational conditions on the energy efficiency of photovoltaic modules operating in Malaysia, J. Clean. Prod. 143 (2017) 912–924, https://doi.org/10.1016/j.jclepro.2016.12.029.

[57] M.F. Umam, Md. Hasanuzzaman, N.A. Rahim, Global advancement of nanofluid-based sheet and tube collectors for a photovoltaic thermal system, Energies 15 (2022) 5667, https://doi.org/10.3390/en15155667.

[58] V.T. Rao, Y.R. Sekhar, Hybrid photovoltaic/thermal (PVT) collector systems with different absorber configurations for thermal management – A review, Energy Environ 34 (2023) 690–735, https://doi.org/10.1177/0958305X211065575.

[59] E. Sakellariou, P. Axaopoulos, Simulation and experimental performance analysis of a modified PV panel to a PVT collector, Sol. Energy 155 (2017) 715–726, https://doi.org/10.1016/j.solener.2017.06.067.

[60] M.S. Hossain, A.K. Pandey, J. Selvaraj, N.A. Rahim, M.M. Islam, V.V. Tyagi, Two side serpentine flow based photovoltaic-thermal-phase change materials (PVT-PCM) system: energy, exergy and economic analysis, Renew. Energy 136 (2019) 1320–1336, https://doi.org/10.1016/j.renene.2018.10.097.

[61] H. Bahaidarah, A. Subhan, P. Gandhidasan, S. Rehman, Performance evaluation of a PV (photovoltaic) module by back surface water cooling for hot climatic conditions, Energy 59 (2013) 445–453, https://doi.org/10.1016/j.energy.2013.07.050.

[62] C. Shen, Y. Zhang, C. Zhang, J. Pu, S. Wei, Y. Dong, A numerical investigation on optimization of PV/T systems with the field synergy theory, Appl. Therm. Eng. 185 (2021) 116381, https://doi.org/10.1016/j.applthermaleng.2020.116381.

[63] M. Chandrasekar, S. Suresh, T. Senthilkumar, M. Ganesh Karthikeyan, Passive cooling of standalone flat PV module with cotton wick structures, Energy Convers. Manag. 71 (2013) 43–50, https://doi.org/10.1016/j.enconman.2013.03.012.

[64] R. Nasrin, M. Hasanuzzaman, N.A. Rahim, Effect of high irradiation and cooling on power, energy and performance of a PVT system, Renew. Energy 116 (2018) 552–569, https://doi.org/10.1016/j.renene.2017.10.004.

[65] H.G. Teo, P.S. Lee, M.N.A. Hawlader, An active cooling system for photovoltaic modules, Appl. Energy 90 (2012) 309–315, https://doi.org/10.1016/j.apenergy.2011.01.017.

[66] A. Nahar, M. Hasanuzzaman, N.A. Rahim, Numerical and experimental investigation on the performance of a photovoltaic thermal collector with parallel plate flow channel under different operating conditions in Malaysia, Sol. Energy 144 (2017) 517–528, https://doi.org/10.1016/j.solener.2017.01.041.

[67] H. Fayaz, N.A. Rahim, M. Hasanuzzaman, R. Nasrin, A. Rivai, Numerical and experimental investigation of the effect of operating conditions on performance of PVT and PVT-PCM, Renew. Energy 143 (2019) 827–841, https://doi.org/10.1016/j.renene.2019.05.041.